UNIVERSITY OF TECHNOLOGY SYDNEY
Faculty of Engineering and Information Technology

MODELLING AND SIMULATION OF HANDOVER IN LIGHT FIDELITY (LI-FI) NETWORK

by

Hieu Danh Huynh

A Thesis Submitted
in Partial Fulfillment of the
Requirements for the Degree

Master of Engineering (Research)

Sydney, Australia

12/2020

Certificate of Original Authorship

I, Hieu Danh HUYNH declare that this thesis, is submitted in fulfilment of the requirements for the award of Master of Engineering (Research), in the School of Electrical and Data Engineering, Faculty of Engineering and Information Technology at the University of Technology Sydney.

This thesis is wholly my own work unless otherwise reference or acknowledged. In addition, I certify that all information sources and literature used are indicated in the thesis. This document has not been submitted for qualifications at any other academic institutions.

This research is supported by the Australian Government Research Training Program.

Production Note:
Signature: Signature removed prior to publication.

Date: 12/12/2020

Acknowledgements

I would like to express my special gratitude to my principal supervisor, A/Prof. Dr. Kumbesan SANDRASEGARAN, for the patience, generous support and immense knowledge he afforded me throughout this study.

A special thanks to my parents who were always supporting and encouraging me with their best wishes.

I would also like to thank to Department of Education and Training for giving me financial support in form of a Research Training Program Scholarship (RTPS) scholarship.

Hieu Danh HUYNH

Sydney, Australia, 2020.

List of Publications

The content of this thesis is based on the following papers that have been published or accepted to peer-reviewed conferences.

Conference Papers

C-1. H. D. Huynh, K. Sandrasegaran and S. C. Lam 2018, 'Modelling and Simulation of Handover in Light Fidelity (Li-Fi) Network', *TENCON 2018 - 2018 IEEE Region 10 Conference*, pp. 1307-12.

C-2. H. D. Huynh and K. S. Sandrasegaran 2019, 'Coverage Performance of Light Fidelity (Li-Fi) Network', *2019* 25^{th} *Asia-Pacific Conference on Communications (APCC)*, pp. 361-66.

Contents

List of Figures

List of Tables

Abbreviation

ADC	Analogue to Digital Converter
ADR	Angle Diversity Receiver
AF	Amplify-and-Forward
AP	Access Point
APS	Access Point Selection
BS	Base Station
CCI	Co-Channel Interference
CCU	Central Controller Unit
CSI	Channel State Information
DAC	Digital to Analogue Converter
DF	Decode-and-Forward
DD	Direct Detection
EGC	Equal Gain Combining
FL	Fuzzy Logic
FOV	Field of View
FR	Frequency Reuse
FSO	Free-Space Optical
IB	In-Band
IM	Intensity Modulation
IR	Infrared
IrDA	Infrared Data Association
JOA	Joint Optimization Algorithm

LAC	Light Fidelity Attocell
LB	Load Balancing
LD	Laser Diode
LED	Light Emitting Diode
Li-Fi	Light Fidelity
LOS	Line of Sight
MAC	Medium Access Control
MIMO	Multiple-Input Multiple-Output
MRC	Maximum Ratio Combining
OBS	Optical Base Station
OPC	Optimum Combining
OWC	Optical Wireless Communications
PD	Photodiode
PDF	Probability Density Function
PF	Proportional Fairness
PPP	Poisson Point Process
QoS	Quality of Service
RF	Radio Frequency
RGB	Red, Green and Blue
SBC	Select Best Combining
SD	Standard Deviation
SDMA	Space-division Multiple Access
SIR	Signal to Interference Ratio
SINR	Signal to Interference plus Noise Ratio
SNR	Signal to Noise Ratio
SOA	Separate Optimization Algorithm
SSL	Solid State Lighting

SSS	Signal Strength Strategy
TDMA	Time Division Multiple Access
UE	User Equipment
VL	Visible Light
VLC	Visible Light Communication
Wi-Fi	Wireless Fidelity

Nomenclature and Notation

Notation	Definition
A	the effective photodetector area
d	the Euclidean distance between AP_i and UE
g	the receiver's optical concentrator gain - gain used to concentrate the received signal of the photodiode detector
$H_{LOS}(0)$	LOS channel gain
$I(0)$	the Lambertian irradiance at the centre of the beam in W/m^2
m	the refractive index
n	order of Lambertian irradiance
n_{rx}	the normal vectors of the receiver plane
n_{tx}	the normal vectors of the transmitter plane
N	the number of users
N_i	users are served by each AP
N^{AP}	the number of AP
R_0	Lambertian radiant intensity - the angular distribution of the radiation intensity pattern
$r_{q,j}$	the rate of j^{th} user when being served by q^{th} AP
$r_1^T, r_2^T, ..., r_Q^T$	rate vectors
T	timeslot T
α	the receiver orientation along the z-axis
β	the receiver orientation along the x-axis

γ	the receiver orientation along the y-axis
ϕ	function angle of irradiance - angle between the transmitter - receiver distance and the vertical axis (from the transmitter)
$\phi_{1/2}$	the half power angle
φ	angle of incidence - angle between the transmitter - receiver distance and the vertical axis (from the receiver)
φ_c	the field of view of the photodiode receiver
$\|\| \ \|\|$	the Euclidean norm operators
$\|R\|_\infty$	the maximum absolute row sum of the matrix R
"."	the inner product

ABSTRACT

MODELLING AND SIMULATION OF HANDOVER IN LIGHT FIDELITY (LI-FI) NETWORK

by

Hieu Danh Huynh

With the demand for faster and secure communication technologies to make our lives better, innovative technologies like Li-Fi (Light Fidelity) are becoming increasingly popular. Li-Fi utilizes Light Emitting Diodes (LEDs) for accomplishing data transmission. This research concentrates around handover algorithms and performance evaluation of a Li-Fi network. Accordingly, the work is outlined in two parts.

Firstly, this research work evaluates the performance of handover algorithms in Li-Fi network. Two handover algorithms are investigated namely, the closest-AP-based algorithm (AP: Access Point) and maximum-channel-gain-based algorithm. Monte Carlo simulations using MATLAB tools are conducted to evaluate handover algorithms and show the impact of User Equipment (UE)'s rotation and movement on handover performance.

Secondly, this research evaluates the performance of a Li-Fi network with multiple beams LEDs on moving UEs. The network performance is investigated in the case of the maximum channel gain. The simulated results show that when the beam angle is 30^o, the Li-Fi system has the best performance in terms of channel gain (hence throughput) by considering its mean and standard deviation (SD) values.

Chapter 1

Introduction

1.1 Research Significance

The mobile data traffic is predicted to exceed 30.6 Exabyte/month in 2020 because of the increasing popularity of smart devices and mobile data services [1]. In addition, due to the shortage of radio spectrum from 300 KHz to 30 GHz, mobile service providers are considering the expansion of the capability of their 4^{th} generation mobile networks and building more Wireless Fidelity (Wi-Fi) hotspots to offload wireless traffic [1].

Moreover, some studies have been conducted on various innovative technologies to enhance the spectral efficiency of existing Radio Frequency (RF) based wireless networks, such as Multiple-Input Multiple-Output (MIMO) techniques [2]. However, due to the continuous increase of wireless traffic, it is anticipated that the current radio spectrum will no longer fulfill the demand of wireless data traffic requirements of the future despite the efforts on numerous recent research in RF communication technologies [2].

The combination of Visible Light Communications (VLC) or Optical Wireless Communications (OWC) technology with small cells deployment is a promising solution to overcome the increasing spectrum shortage in wireless communication, and open the door for new network to be released which is called Light Fidelity (Li-Fi).

Although there are some studies on the handover in Li-Fi, a transparent mobility model for mobile User Equipment (UE) devices lacks in most of those studies except the research work in [3]. Additionally, all existing mobility models of mobile UE

devices assumed that the device is always facing vertically upward. However, it might not be applicable in Li-Fi networks because Li-Fi devices can be rotated while in movement [3].

1.2 Research Contributions

The first part of this research aims to provide a basic modelling of handover in downlink Li-Fi Attocell (LAC) networks with the consideration of mobility and rotation of UE device. This simulation modelling is extended from the mobility model framed in [3].

When UE is rotating around three standard axes (x, y, and z), the random waypoint and rotation models were used to evaluate the Signal to Interference Ratio (SIR) and handover decision [5]. SIR is the quotient between the average received modulated carrier power S and the average received co-channel interference power I. With the entities calculated, we could determine the performance of a typical UE while it is in movement or performing rotating motion. Along with this, we can also ensure that seamless communication is maintained during the handover process.

In addition, some studies were conducted about handover performance in Li-Fi networks but there was only a limited analysis of multiple beams Light Emitting Diodes (LEDs) considered in existing literature. Multiple beams LEDs techniques are expected to improve the coverage of a Li-Fi networks. The second part of this research focuses on the handover process of a UE moving in multiple beams LEDs scenario in a square network area.

1.3 Research Aims and Objectives

The aims of the research are:

i. Investigating handover algorithms while UE is moving and rotating in the Li-

Fi network.

ii. Investigating the impact of beam angles of multiple beams LEDs during the handover process in the Li-Fi network.

The objectives of the research is to investigate the performance of Li-Fi through:

i. Modelling single beam and multiple beams LEDs in the Li-Fi network environment.

ii. Simulation of the handover algorithms in the Li-Fi network (single beam and multiple beams LEDs).

iii. Statistically, analysis of collected data to evaluate the performance of handover algorithms used in the Li-Fi network.

1.4 Research Methods

There are three research methods that are used in this research:

i. The first method is an experimental method [6] which simulates a Li-Fi network in the MATLAB environment. By utilizing some built-in functions in MATLAB and giving random waypoint and rotation model of UE device as inputs, the performance are evaluated from the collected raw data.

ii. The second method is the analytical method [7] which uses Excel to analyze the results and data statistically. By doing the statistical analysis, the performance of each handover algorithm is investigated.

iii. The third method is the correlational research methodology [8] which identifies appropriate handover algorithms for the Li-Fi network. In order to do that, the comparison is made based on the advantages of all simulated algorithms and then finding out the relationship between these algorithms.

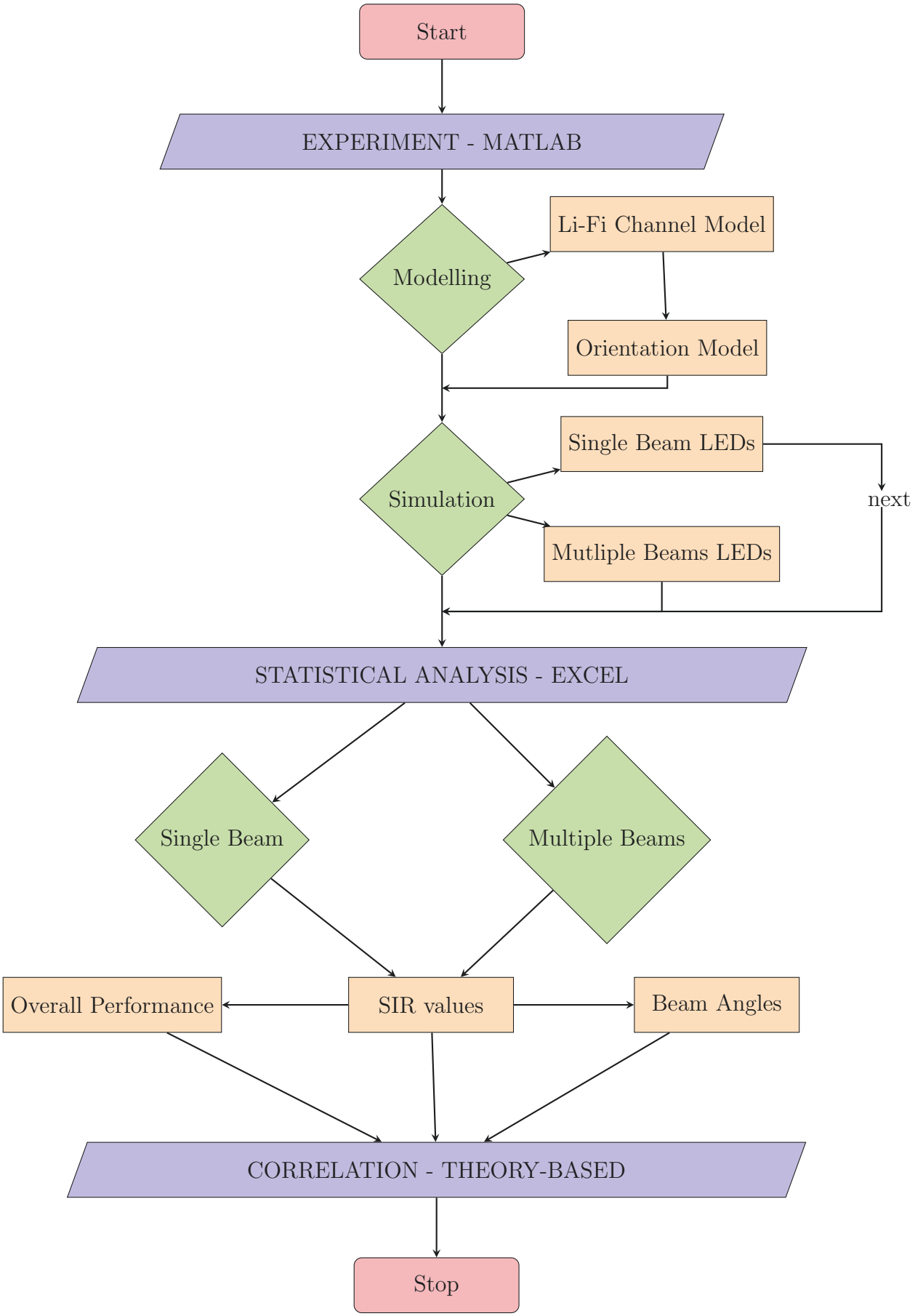

Figure 1.1 : Research Method Diagram

1.5 Thesis Layout

This thesis is organized in the following way.

- Chapter 1 introduces the significance of the research, research contributions, research aims, and objectives, research methodology, thesis layout, and summary.

- Chapter 2 provides background information about the Li-Fi networks which comprises of, the definition, evolution, system operation, system architecture, advantages and disadvantages of Li-Fi network, LAC network, downlink transmission and handover description.

- Chapter 3 presents the literature review of handover algorithms, load balancing, multiple beams and intercell interference.

- Chapter 4 presents the modelling and simulation results including: Li-Fi channel, Geometric orientation model, single beam and multiple beams LED models.

- Chapter 5 contains the performance analysis of the single beam LEDs model.

- Chapter 6 contains the performance analysis of the multiple beams LEDs model.

- Chapter 7 describes the conclusions, limitations and future works.

1.6 Summary

The research significance, research aims, and objectives, research method, plus the thesis layout are presented in this chapter. The research significance mentioned the necessity of this research by filling the existing research gap. There were two research aims and three research objectives were listed in the next part. Additionally, there different research methods were also described followed by the visualized flow chart. Finally, the layout of this thesis was listed including the introduction of seven chapters.

Chapter 2

Background

2.1 Definition

Li-Fi is an OWC technology where LEDs are used for data transmission. This technology provides a different type of wireless communication system, which is considered as the optical version of Wireless Fidelity (Wi-Fi). In optical communication, the information is transmitted between two different locations by using electromagnetic radiation in the optical spectrum [2].

A Li-Fi network uses LED bulbs which are similar to those that are currently used in our daily life. A chip inside the LED bulb is used to modulate the light gradually for transmitting optical data. Li-Fi data is transmitted by the LED bulbs and received by a photodetector [9].

The optical frequency carrier for Li-Fi information transmission and illumination uses the visible light which lies in the frequency range between 400 THz (780 nm) and 800 THz (375 nm). In addition, fast pulses of light are utilized to transmit data wirelessly [9].

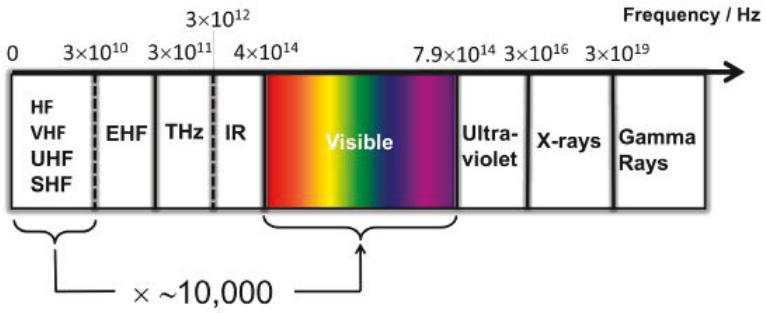

Figure 2.1 : The total frequency bandwidth of the electromagnetic spectrum [11].

The optical spectrum used in OWC includes the Infrared (IR) and Visible Light (VL) bands [10]. Figure 2.1 shows that the total frequency bandwidth of the optical spectrum is several hundred THz, which is much broader than any deployed RF spectrum. Hence, the spectrum bandwidth could be possibly utilized for future high traffic demands [11]

There are several optoelectronics devices that are used to support the high speed OWC such as LED, Laser Diode (LD), and Photodiode (PD). These devices are capable of efficiently converting optical to electrical signals and vice versa with sufficient wide modulation bandwidth [12].

Free-space transmissions in a long distance from point to point [12] or Free-Space Optical (FSO) communication has been considered as one of the applications of OWC.

2.2 History

In the 1960s and 70s, optical light based communications had been applied for military purposes due to the emergence of security characteristics of FSO technologies.

Gfeller and Bapst in [13] are the pioneers for developing OWC short-range indoor

applications focusing on the data rate target of 100kbps for diffused IR radiation communication systems.

In 1993, based on the IR technology development, Barker and his associates in [14] found the Infrared Data Association (IrDA) by formulating wireless IR communication protocols among electronic devices.

Thereafter, the Solid State Lighting (SSL) has become popular along with the necessary demand for energy-efficient white-LED [15].

The replacement of all traditional lighting equipment, such as fluorescent lamps, by LED-based lighting infrastructures is our expectation in future. And it also provides a new opportunity to transfer the wireless communication networks to future lighting networks, which is also known as VLC [16].

2.3 Evolution

Due to the shortage of radio spectrum below 10GHz, the wireless communication system has considered the radio spectrum above 10GHz. However, communication in higher frequencies also has some problems such as an increase in the path loss, signal blockages, fading and shadowing [36].

Li-Fi is immune to these propagation effects and hence can be utilized in indoor scenarios by using light from LEDs for high-speed, networked and mobile communication [11] in a similar manner as Wi-Fi [9]. Moreover, the Li-Fi system could be built on the existing lighting infrastructures.

A network consisting of multiple Li-Fi APs is called as the LAC network [17]. A LAC network also has an ability to minimize interference and provide fully networked wireless connectivity with multiuser access and handover [11].

2.4 System Operation

Fig. 2.2 shows the components of a Li-Fi system. One of the key elements of this communication system is a high brightness red, green and blue (RGB) LED, which plays the role of a communication source. This type of LED can increase data rates by mixing the base colors instead of using a color converting chemical [39] & [40].

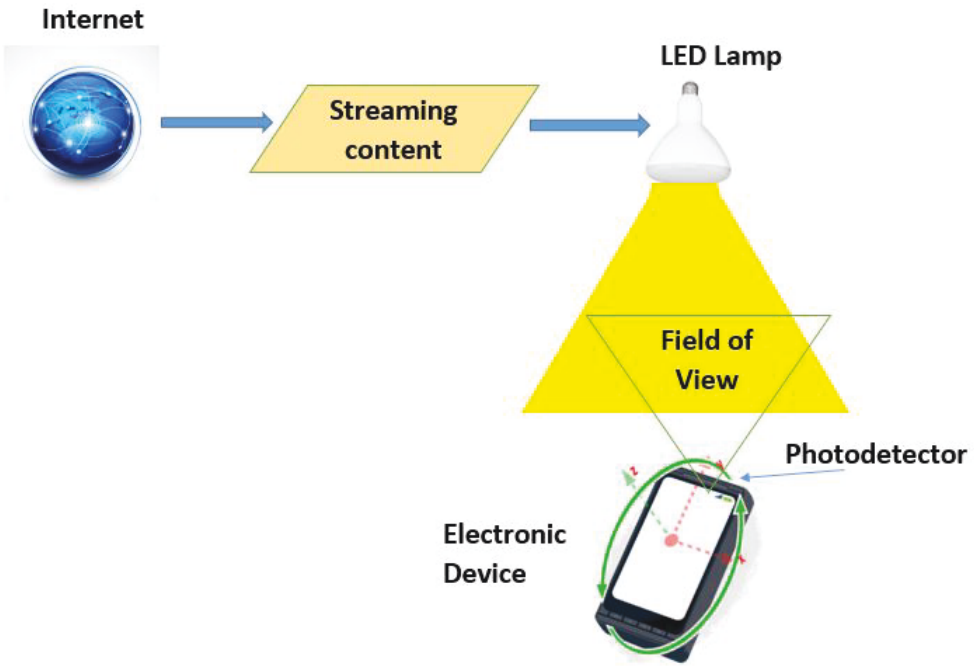

Figure 2.2 : Li-Fi network operation.

There is a transmitter chip integrated into the LED involving digital to analogue converter (DAC), and the chip package (size 5mm x 6mm) is shown in Fig. 2.3 with the coin alongside to give the scale [11].

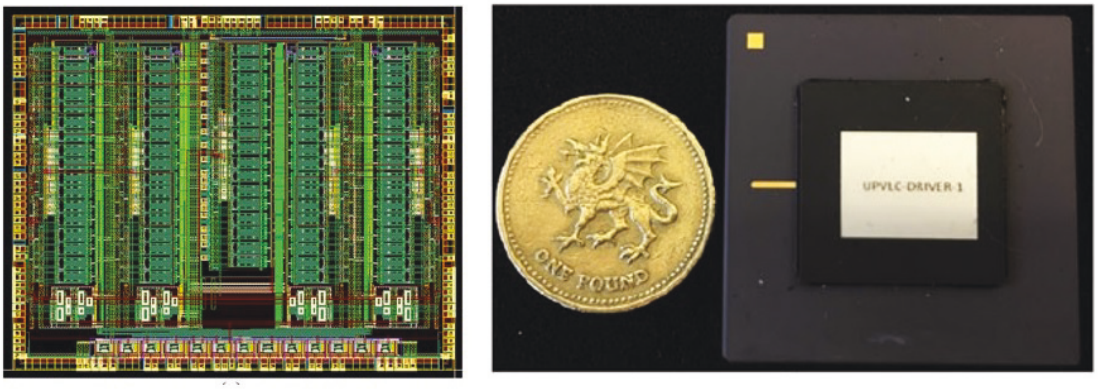

Figure 2.3 : The layout and the package of Li-Fi transmitter chip [11].

As the LED's switching speed is less than 1 μs, human eye cannot detect the flashing of the LED light and light source seems to be persistent. A binary "1" and "0" have been generated by switching LED on and off. This imperceptible on-off action allows information transmission utilizing binary codes. In addition, we can get sequence of 1s and 0s by changing the LED's flickering rate. Moreover, light frequencies might change with each frequency encoding a different colour by using an array of LEDs for parallel data transmission or a mixture of Red, Green and Blue (RGB) LEDs.

At the receiver part, there is a photodetector that is connected to the electronic device (Fig. 2.2). The purpose of this photodetector is to encode the digital data stream. There is a receiver chip to amplify and process data with the analogue to digital converter (ADC). Fig. 2.4 shows the receiver chip's layout and package. The size of a receiver chip is of the order of 3mm x 3mm [11].

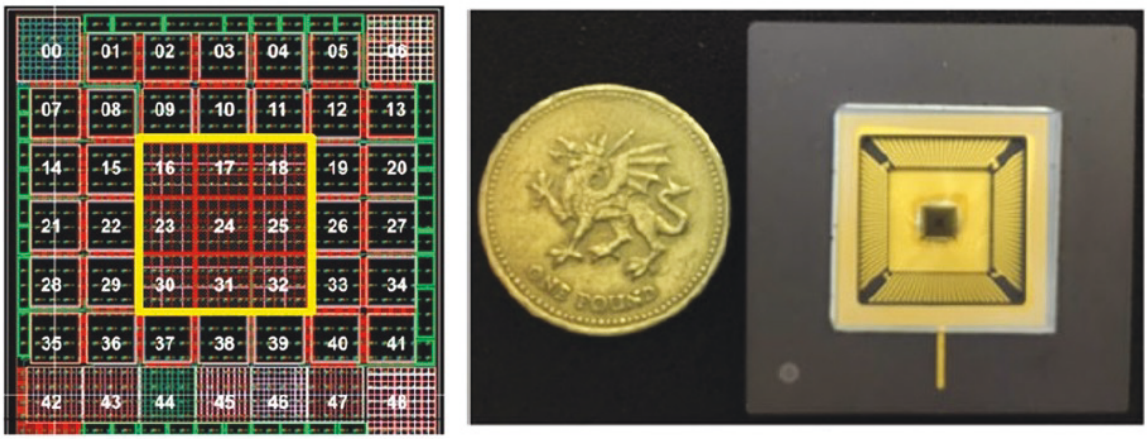

Figure 2.4 : The layout and the package of Li-Fi receiver chip [11].

2.5 System Architecture

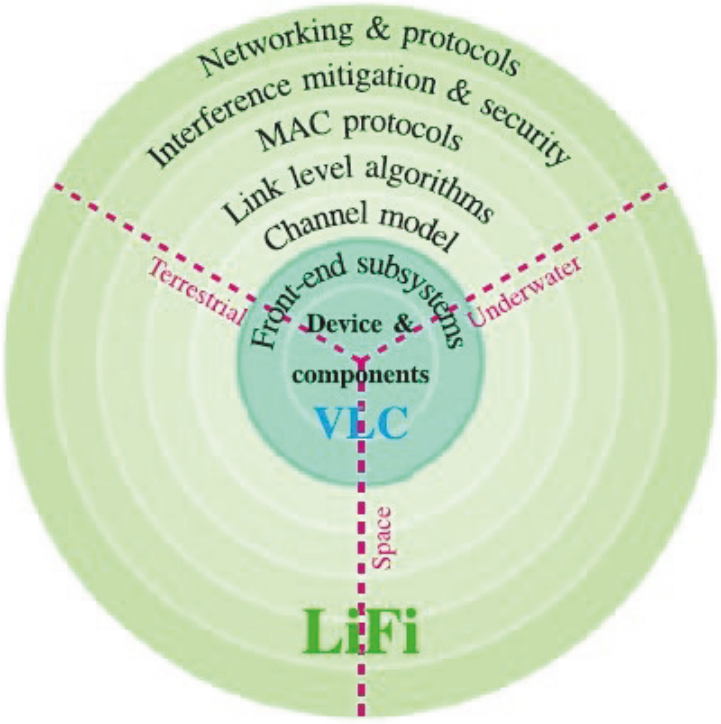

Figure 2.5 : The main building blocks of Li-Fi and its application areas [11].

The principal building blocks of Li-Fi are shown in the Fig. 2.5 with its application areas. At the core, there are devices and components of LEDs and single-photon avalanche diodes, which are embedded in optical front-end subsystems [18].

At the physical layer, there is a requirement for precise channel models when light is transmitted from point A to point B. By fulfilling this requirement, this layer is used to model link margins, and establish the channel's coherence bandwidth and the co-channel interference (CCI) [18].

In the link layer, a new theoretical framework was adapted to determine the channel capacity and maximize the data throughput. The channel capacity (including the Gaussian noise) with low Signal to Noise Ratios (SNR) was determined in [18] to match this requirement.

The subsequent layer has new Medium Access Control (MAC) protocols playing a role as the Li-Fi physical layer in order to enable multi-user access. Interference mitigation and security techniques are also used to ensure the system throughput remains at the fairness or high level [18].

Lastly, the integration of the LAC network into software-defined networks is one of the requirements for the last layer - network and protocols where the networks are managed separately by the control and data planes and network virtualization [18].

2.6 Advantages and Disadvantages of Li-Fi

Advantages of Li-Fi There are several advantages of using Li-Fi. Firstly, as Li-Fi works on visible light technology, the LEDs used for illumination is also used as the Access Points (AP) to transmit data. Secondly, this technology is available for implementation where we have LEDs installed for illumination purposes. Thirdly, because light cannot pass through concrete structures, Li-Fi is only available to the

users within a room or specific space. Hence, it cannot be breached by users in other rooms or spaces. Moreover, this advantage also leads to a decrease in interference between neighbouring networks in different rooms. Next, as Li-Fi uses a higher bandwidth than other wireless system, there is more available bandwidth for this new communication technology. Unlike the electromagnetic radiation in RF signals, Li-Fi has less effect on human health.

In addition, transmission directionality is obtained by beam-forming techniques with multiple antennas in RF-based communication systems, while VL sources and detectors provide directionality with cost-effective optics [2].

Disadvantages of Li-Fi When light cannot penetrate through walls, Li-Fi offers a very limited range and provides coverage in a shorter distance then Wi-Fi.

In addition, there is an issue with compatibility of existing device which has to be modified to enable Li-Fi receiving functions.

2.7 Li-Fi Attocell Network (LAC)

The small-cell network is combined with VLC techniques to establish a fully networked VLC system where multiple existing lighting infrastructures can be used as VLC APs. In other words, it is called the LAC network, where it is able to transmit bi-directionally, serve multiple users with a single AP, and support mobility [19]. In this case, there are two requirements for a LAC network including roaming and smooth handover, and controlling CCI in a minimum level.

In terms of flexibility and mobility aspects, VLC only offers point-to-point links which has the limited coverage when compared to RF wireless systems. One of the solutions to overcome this issue is providing multiple VLC infrastructures as the LAC network - a networked system [11, 19].

The LAC concept network is illustrated in Fig. 2.6. Each VLC infrastructure can be considered as an Optical Base Station (OBS) where a number of UEs are served within its local coverage area [2].

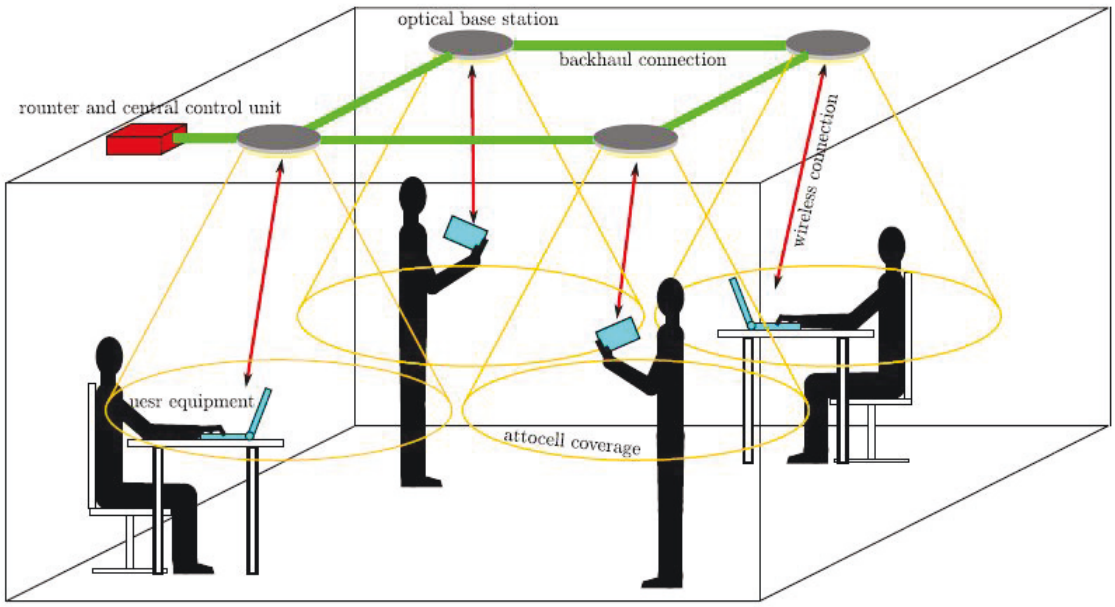

Figure 2.6 : The concept of Li-Fi attocell network [2].

A LAC network is expected to have a cellular system's full functionality due to the benefits offered by VLC technology [19]. These advantages are listed below.

Firstly, in VLC technology, typically, the light source radiates optical power into a specified direction with a specified beam-width. Therefore, the VL signal's radiation can be confined within a limited region, typically the area underneath the light source. In general, this characteristic is totally different from omnidirectional antennas radiating RF signal to all directions [2].

Secondly, LAC networks could be implemented by modifying existing lighting networks [4]. No new equipment needs to be installed in the ceiling. This is important in several cases like heritage buildings.

Thirdly, an extra layer of heterogeneous networks with zero interference with existing infrastructure could be added [2].

The spectral efficiency perspective of VLC technology leads to the combination of using unlicensed spectrum and cell densification, which makes the LAC network a promising future wireless access network [2].

Therefore, LAC networks should have a smaller cell size than a mmWave communication system. It means a LAC system can achieve a much higher data capacity per unit area [11]. Deploying the LAC network as an extra layer in a future heterogeneous network is a very promising solution to offload the significantly increased mobile data traffic in the future wireless communication networks [2].

2.8 Downlink Transmission

While the downlink transmission is transmitted from a Base Station (BS) to a UE in the cellular networks, it is forwarded from an OBS to a Li-Fi UE in LAC systems [20]. Figure 2.7 describes a basic setup for a LAC downlink system [2]. Only physical layer in the LAC downlink system is considered in this research.

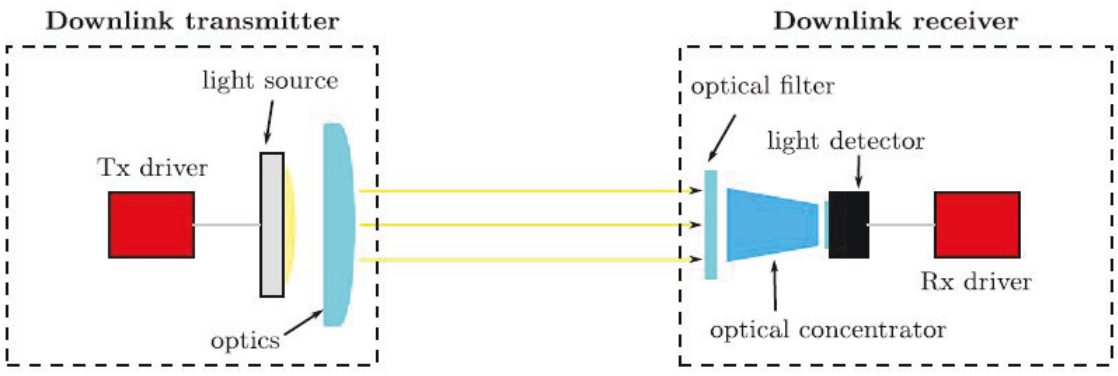

Figure 2.7 : Key components in a LAC downlink transmission system [2].

The downlink system in LAC and RF network is very similar except for the front-end elements. RF cellular system coverts the modulated electrical signal to the RF electromagnetic wave signal in a single step. But there are two steps involved in the LAC downlink system for performing this conversion.

Firstly, the transmitter's front-end elements will convert the modulated electrical signal to a light signal, and then receiver's front-end elements will convert the transmitted light signal back to the modulated electrical signal. These two steps are shown in the Fig. 2.7 [2].

The Intensity Modulation (IM) with Direct Detection (DD) techniques are used in the front-ends of the LAC downlink transmission channel due to its appropriateness [2]. The key advantages of using IM with DD techniques are reducing the effects of direct current wander and ambient light as well as achieving high spectral efficiency [22].

2.9 Handover Definition

Handover is the process of transferring the user control from the current serving AP to a different AP with the assurance of seamless wireless transmission signals [23].

There are two reasons for a handover to occur. Firstly, UE is moving out of the existing coverage area of the serving AP and into the adjacent AP's coverage area. Secondly, the current cell is overloaded, or the signal quality received is poor because of fading or interference effects.

Handovers that occur between APs within a network that are called horizontal handovers. In other cases, it is vertical handover when it occurs between APs in different networks [24].

In general, there are two types of handover schemes: soft and hard handover [2].

Hard handover happens when there is a disconnection between UE and the current

AP prior to connect to the new AP. This scheme is simple due to its lower hardware requirements [23]. One drawback of this scheme is that the service will be interrupted during the transition time. All handovers in 2G, 4G and 5G are hard handovers.

In contrast, there is no interruption in the soft handover process because UE keeps its connection with the existing AP until the new connection with the new AP is established. This requires the cooperation between APs and extra hardware configurations.

In the OWC, the soft handover is recommended for use due to its advantage. The handover frequency in the LAC network is high due to its small cell size (LAC network possesses the smallest cell size compared to other types of small-cells), this handover process might satisfy the requirement of system throughput and Quality of Service (QoS). This small cell size causes a high number of handover sessions and ping-pong effect among moving UEs so the novel handover algorithms should be invented to overcome these problems [24]. In terms of QoS, it refers to the overall communication performance that the LAC users experienced.

In addition, OBSs are physically in close proximity to each other causing the high handover frequency in a LAC network. Moreover, it implies that the backhaul constraints for centralized control and cooperation among OBSs are relatively easier to fulfil than the case of RF cellular systems. [2].

2.10 Conclusion

In this chapter, the Li-Fi definition is described together with its history of development and evolution. In order to understand Li-Fi networks, the terms OWC, LED bulbs and optical frequency carrier are presented. In the history part, some OWC technologies were used in the past from different researchers are the fundamental approach for Li-Fi development in future. In the evolution part, the shortage of

radio spectrum below 10GHz is mentioned leading to the commencement of new technology named Li-Fi - an optical version of Wi-Fi.

Next, Li-Fi system operation and architecture are shown with an overview of Li-Fi network operation, transmitter and receiver chip, principle building blocks of Li-Fi, and its application areas. In addition, the pros and cons are also shown in the following parts. There are two disadvantages of Li-Fi network. They are the limited range and short distance coverage of Li-Fi network and compatibility with new Li-Fi enabled personal device. In terms of its advantages, Li-Fi uses LEDs bulbs for illumination and communication which is convenient and it has higher security. The descriptions of LAC network, downlink transmission and handover are presented in the next three parts. LAC network related to Li-Fi where LEDs are used as the AP is also explained. Only downlink transmission is considered in this research while assessing the handover process happening between the network and UE devices.

Chapter 3

Literature Review

This chapter presents a literature review of Li-Fi networks concepts that are relevant to this research. This includes handover algorithms, load balancing, multiple beams and intercell interference. The ideas described in this chapter are used in Chapter 4, 5 and 6.

3.1 Handover Algorithm

In [9], the AP selection algorithm in the central controller unit (CCU) was proposed by considering both the maximum received signal and the APs' traffic to maximize system throughput. A CCU controls all APs in a Li-Fi network which has already been connected via a wired network.

By applying the feedback procedure, this CCU collects the Channel State Information (CSI) from all APs and receivers. Assuming that the number of AP is N^{AP} and the number of users is N in the network area and N_i users are served by each AP, i $\in$ (1, 2, . . . , N^{AP}).

When the $(N+1)^{th}$ user who is a new user joins the networked area, the request is broadcasted to all APs. The APs' set is denoted by $\boldsymbol{Q}$ with Q elements when this $(N+1)^{th}$ user has its Field of View (FOV) is included in that set.

Each of the Q APs is selected by the $(N+1)^{th}$ user but only one of those Q APs' set provides the highest throughput.

Based on the new user's CSI and the APs in that new user's FOV, Q possible rate vectors which correspond to the Q APs in the FOV of that new user $(N+1)^{th}$ is

calculated as follows:

$$r_q = [r_{q,1} \quad r_{q,2} \quad ... \quad r_{q,N+1}] \tag{3.1}$$

where

- q ∈ Q
- $r_{q,j}$ is the rate of j^{th} user

  > 0 if that user is connected to q^{th} AP

  $= 0$ if that user is not connected to q^{th} AP

After calculating all rate vectors, the matrix R is calculated as follows:

$$R = [r_1^T, \quad r_2^T, \ ... \ , r_Q^T]^T \tag{3.2}$$

where

- $r_1^T, r_2^T, ..., r_Q^T$: rate vectors

After the q responses to the matrix $\|R\|_\infty$, the best AP is chosen based on the maximum absolute row sum of the matrix. The best AP provides both network load balancing (LB) and maximum throughput to users. The maximum absolute row sum of the matrix R is shown as follows:

$$\|R\|_\infty = \max_{1 \le q \le Q} \sum_{j-1}^{N_q+1} r_{q,j} \tag{3.3}$$

where

- $\|R\|_\infty$: the maximum absolute row sum of the matrix R

- $r_{q,j}$: the rate of j^{th} user

The drawback of this technique is regardless of the load of AP causing the unbalance between APs: users may connect to an overloaded AP and leave other APs idle. By considering the load balancing among APs and to provide a better users QoS, a new metric for AP selection in Li-Fi cellular networks with arbitrary receiver orientation was proposed [9].

3.2 Load Balancing (LB)

Some studies about load balancing (LB) methods in Li-Fi were conducted in [25], [26], [27], [28] and [29].

Load balancing technique is applied when there are more than one networks covering the same areas in order to avoid overlapping between these networks.

In [25], in order to maximize the proportional fairness (PF) index of all users to solve the problems related to the resource allocation and coordination, there is a need for optimizing the power allocation of the hybrid Li-Fi/Wi-Fi network under the constraint of common backhaul. The Li-Fi and Wi-Fi backhaul system model is shown in the Fig. 3.1.

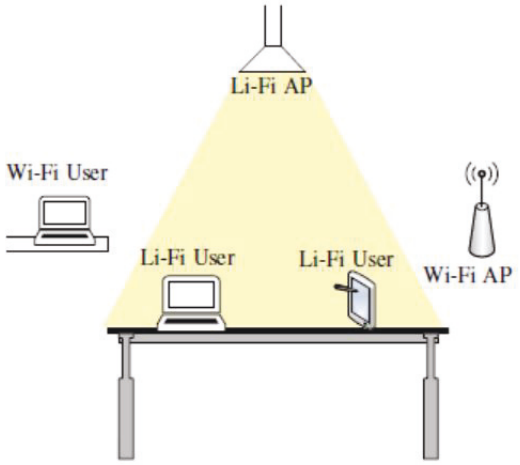

Figure 3.1 : Li-Fi and Wi-Fi backhaul system model [25].

More specifically, the rate and power allocation algorithms are used to guarantee the maximized values of PF among all users are applied in the downlink scenarios only.

In the case of low backhaul capacity, similar data rates can be shared among Li-Fi and Wi-Fi users. Otherwise, the Li-Fi users might have higher data rates than the Wi-Fi users by taking advantages of this condition.

In [26], two dynamic LB schemes in Li-Fi and RF hybrid network are proposed: Joint Optimization Algorithm (JOA) and Separate Optimization Algorithm (SOA). These algorithms are used to jointly and separately optimize the AP assignment and resource allocation, respectively. The following figure shows the schematic diagram of this proposed model.

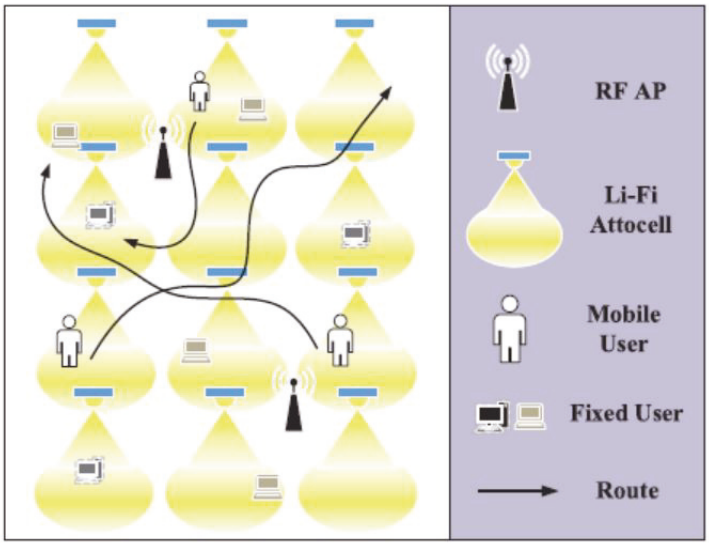

Figure 3.2 : Schematic diagram of the system model [26].

Both algorithms provide optimized fairness coefficient and data threshold to achieve the maximized QoS. The research work in [26] shows that in a typical indoor environment, over 90% of users in JOA achieve the maximum QoS which is 1.3 times larger than that in SOA and the JOA also provides the medium data rate 1.5 times higher than the SOA does. In terms of LB, SOA has a better trade-off between performance and complexity than JOA.

In [27], [28] and [29], the Fuzzy Logic (FL) was used to determine a user's throughput based on CSI.

In [27], a two-stage Access Point Selection (APS) method was suggested for Li-Fi and Wi-Fi hybrid networks, which is shown in Fig. 3.3. Firstly, the algorithm determines which users require service from Wi-Fi, and then assigns the remaining users to a homogeneous Li-Fi network. In this stage, the priority of access the Wi-Fi of users is ranked by applying the Fuzzy Logic (FL) concept. Secondly, the Signal Strength Strategy (SSS) or LB is applied with the proposed method named the Fuzzy Logic-SSS (FL-SSS) or Fuzzy Logic-LB (FL-LB) correspondingly.

Figure 3.3 : Schematic diagram of an indoor hybrid Li-Fi and Wi-Fi network [27].

Based on the experimental results, it is shown that the proposed method achieves a near-optimal throughput with the complexity was reduced significantly. And the FL-LB outperforms the FL-SSS with a slight increase in complexity and the FL-LB can improve the network throughput by 24% and 11% when compared to SSS and LB respectively.

In [28], a dynamic LB scheme which is based on FL was proposed to prevent the handover effects in Li-Fi/RF hybrid network (Fig. 3.4).

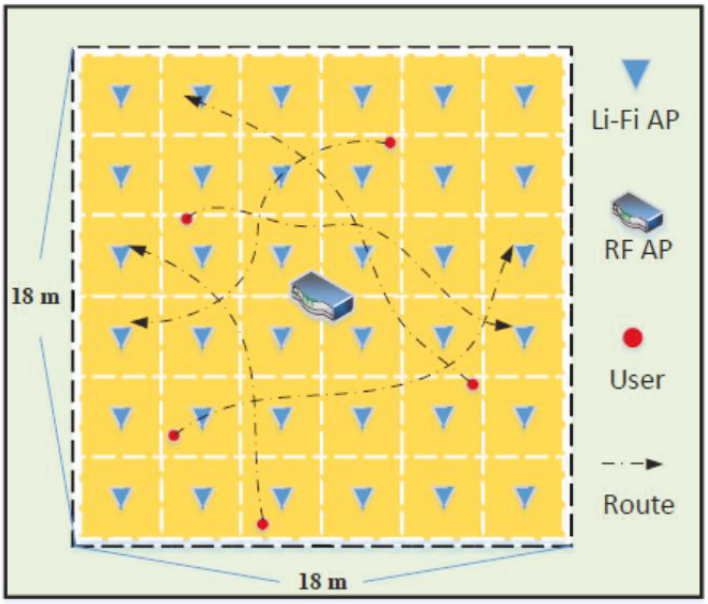

Figure 3.4 : Simulation Scenario of Li-Fi/RF Hybrid Network [28].

In the proposed algorithm, the speed and average Signal to Interference Noise Ratio (SINR) of users who are measured in order to allocate users which have high speed or are experiencing transient shadowing effect to suitable APs, and also reduce the ping-pong handover pattern. The research work in [28] shows that this dynamic LB scheme which is based on FL has lesser data rate loss than the traditional LB algorithms, and both QoS and data rate of users have improved 40%.

In [29], a two-stage APS method was proposed for hybrid Li-Fi and RF networks. This model is shown in Fig. 3.5.

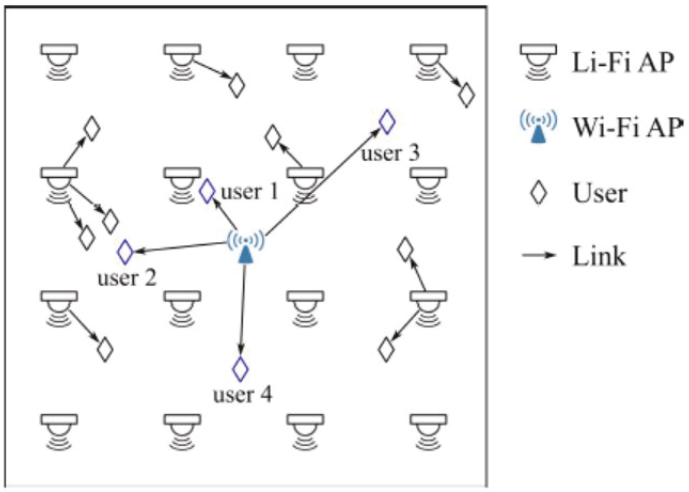

Figure 3.5 : Paradigm of an indoor hybrid Li-Fi/RF network [29].

Firstly, users are served by the RF system and then the remaining users are assigned to the Li-Fi network. By applying this method, the limited resource of RF system is exploited and the overall network performance is also improved.

In [30], the arbitrary receiver orientation is considered to determine the user's SINR and traffic of APs.

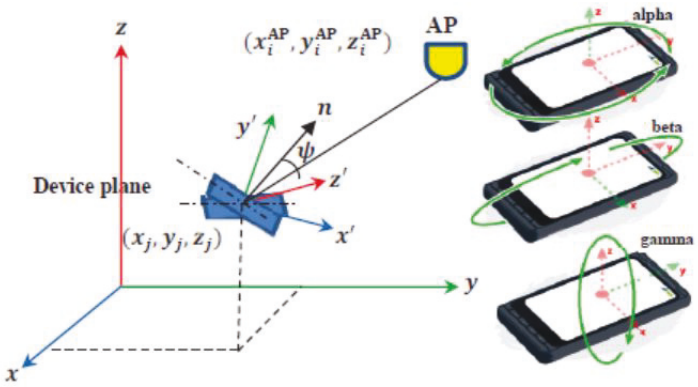

Figure 3.6 : Modelling of device orientation based on rotations in three axes [30].

A new metric for the selection of APs to provide a better QoS for users with arbitrary

receiver orientation is proposed in Li-Fi cellular networks by applying the LB among APs. The performance is evaluated based on three different metrics: user average throughput, satisfaction level, and fairness index in the models of users' orientation. The research work in [30] shows that the proposed method has a better performance compared to the signal strength technique, especially when the number of users or the requested data rate rises.

3.3 Multiple Beams

There are several studies related to multiple beams in the Li-Fi network.

In [31], the angle diversity transmitters are researched to improve coverage areas and this network is shown in the following figure.

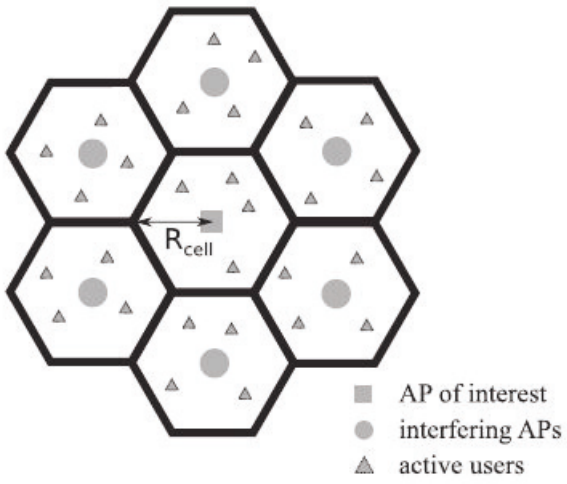

Figure 3.7 : The layout of a 7-cell attocell network [31].

By applying an angle diversity transmitter, the research work in [31] shows that when transmitters have multiple LED elements (37 elements), the spectral efficiency is 26 times higher. It also shows that the optical Space-division Multiple Access (SDMA) system outperforms the optical Time Division Multiple Access (TDMA) benchmark

system when considering system performance. It was also proved that in [31] the optical SDMA system is good in terms of the user positioning errors (about 14%) compared with other practical state-of-the-art indoor positioning techniques.

In [32], in order to increase the AP coverage range, the dynamic beam and luminaire control are applied (Fig. 3.8).

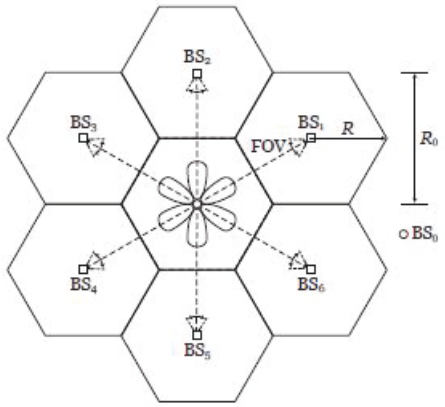

Figure 3.8 : Hexagonal cellular layout of seven attocells [32].

Two bandwidth allocation methods, including the Frequency Reuse (FR) and In-Band (IB)) are used to divide the system bandwidth into two parts: the access and backhaul links for both relaying protocols: Amplify-and-Forward (AF) and Decode-and-Forward (DF). The research work in [32] shows that the performance depends especially on the emission semi-angle of the auxiliary LEDs which are used for the AP-to-AP links in the downlink. It also shows that for either FR or IB methods, DF relaying outperforms AF relaying when the emission semi-angle is larger than 25^0.

3.4 Intercell Interference

There are several studies related to inter-cell interference.

In [33], a very close approximation to co-channel interference is reachable by applying the Fourier analysis (Poisson summation) in attocell networks. It applies for both single and two dimensions. In addition, in order to provide upper bounds for interference, a high degree of accuracy in calculating interference power is proposed when applying this characterization in attocell networks with any given height to inter-LED separation ratio. In addition, the Fourier analysis method can be applied for the case of the user PDs that have limited FOVs by using the interference characterization.

In [34], the statistical-equivalent transformation of the SINR is applied to determine the coverage probability for saving energy and minimizing the co-channel interference in multi-user VLC networks (Fig. 3.9).

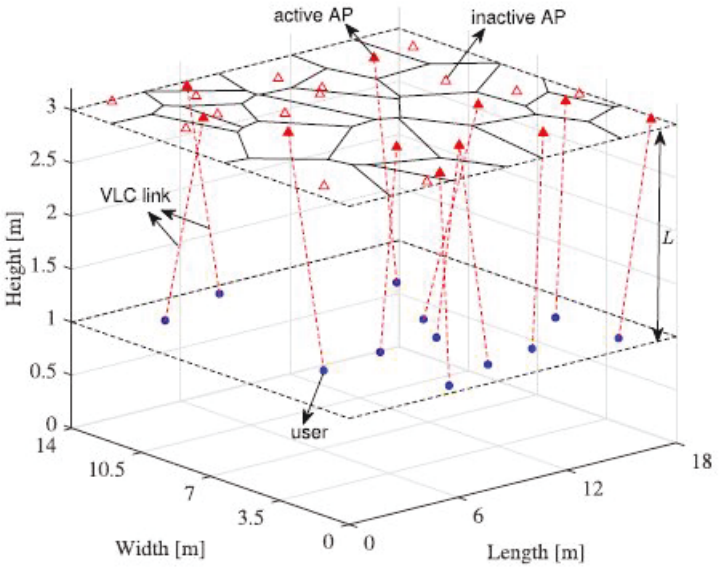

Figure 3.9 : Three-dimensional Voronoi cell formation in the Li-Fi network [34].

In this case, by operating the AP sleep strategy in underloaded and general networks, the APs' idle probability is evident. When the AP density is smaller than the user density, the homogeneous Poisson Point Process (PPP) applied for active APs is

valid. In addition, the PPP also produces the close coverage results to the exact ones. In the multiuser VLC network, if the noise level of the typical receiver is approximately -117.0 dBm [34], the SINR values are approximated by the SIR when analyzing the simplified coverage performance.

In [35], the Angle Diversity Receiver (ADR) is used to mitigate interference based on four methods: Select Best Combining (SBC), Equal Gain Combining (EGC), Maximum Ratio Combining (MRC) and Optimum Combining (OPC). The research work in [35] concluded that in terms of SIR performance, by using OPC to nearly achieve the interference-free systems, the system using ADR outperforms a single-PD receiver system. However, the knowledge of CSI is required in all-optical APs in the network while applying OPC. In contrast, MRC and SBC only require the knowledge of CSI from the desired cell and both of them also have better performance than a single-PD receiver. In addition, MRC and SBC can provide better SINR performance in the double-source cell configuration mode.

3.5 Conclusion

In this chapter, the literature review focuses on the handover algorithms, load balancing, multiple beams, and intercell interference. Firstly, the handover algorithms in central controller unit that select an AP to maximize the system throughput are discussed. Secondly, load balancing methods are used to maximize the proportional fairness index of all users, AP assignments and resource allocation, CSI. Next, multiple beams are used to improve coverage areas by applying the angle diversity transmitter. Lastly, regarding the intercell interference, some studies such as Fourier analysis, the statistical-equivalent transformation of the SINR and the angle diversity receiver are used to provide a very close approximation to co-channel interference in attocell networks for both one and two dimensions, determine the coverage probability for saving energy and minimizing the co-channel interference

in multi-user Visible Light Communication (VLC) networks and mitigate interference, respectively.

Chapter 4

Modelling and Simulation

This chapter contains a description of modelling and simulation of Li-Fi network used in this work including the Li-Fi channel model, orientation model and mobility model.

4.1 Li-Fi Channel

The irradiance distribution of a LED source is illustrated in Fig. 4.1 :

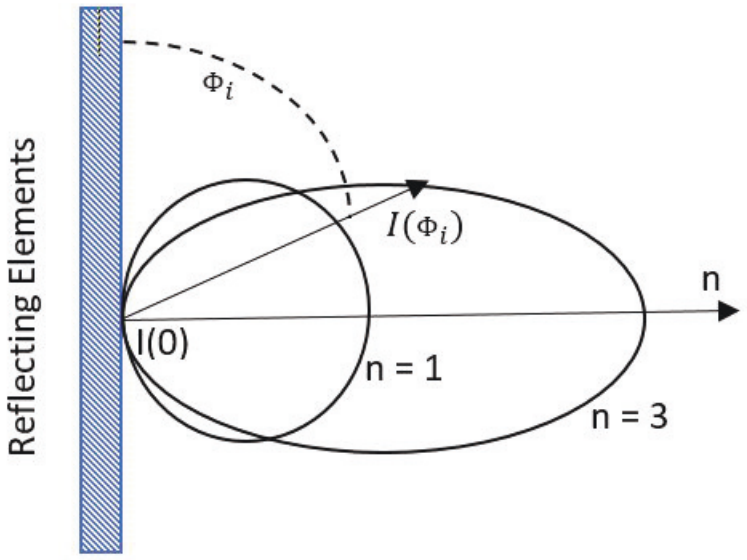

Figure 4.1 : Lambertian emission pattern for mode n [36].

The Lambertian irradiance is defined as [37]:

$$I(\phi_i) = I(0)cos^n(\phi_i) \tag{4.1}$$

where

- I (0) is the Lambertian irradiance at the centre of the beam in W/m^2
- ϕ is the viewing angle of irradiance
- n is the Lambertian irradiance order and it is calculated as follows [37]:

$$n = -\frac{1}{\log_2 cos(\phi_{1/2})} \tag{4.2}$$

where $\phi_{1/2}$: the half power angle.

Lambertian radiation pattern is expressed as [37]:

$$R_0(\phi) = cos^n(\phi)\frac{n+1}{2\pi} \tag{4.3}$$

The average power ratio between received and transmitted signal is defined as [11].

$$H_{LOS} = \begin{cases} \frac{A}{d^2} R_O(\phi) cos(\varphi_i) & 0 \leq \varphi_i \leq \varphi_c \\ 0 & \varphi_i > \varphi_c \end{cases} \tag{4.4}$$

And the channel gain at the receiver includes the optical filter gain T_s and optical concentrator g(φ_i) integrated in the photodetector

$$H_{(receiver)} = \begin{cases} \frac{A(n+1)}{d_i^2 2\pi} cos^n(\phi_i) T_s \mathrm{g}(\varphi_i) \cos(\varphi_i) & 0 \leq \varphi_i \leq \varphi_c \\ 0 & \varphi_i > \varphi_c \end{cases} \tag{4.5}$$

where

- A: the effective photodetector area (m^2)

- n: Lambertian order
- d_i: the Euclidean distance between AP_i and UE (m)
- ϕ_i: the radiance angle with respect to the z-axis (vertical) on the transmitter plane for AP_i
- φ_i: the incidence angle with respect to the z-axis (vertical) on the receiver plane for AP_i
- T_s: optical filter gain of the receiver
- φ_c: Field of View (FOV) of the receiver
- g(φ_i): the receiver's optical concentrator gain

4.2 Geometric Orientation Model

Three angles: α, β and γ are used to specify the receiver orientation along the z, x and y-axis respectively [5]. Fig. 4.2 describes the UE orientation model using the three axes in a cartesian coordinate system [36].

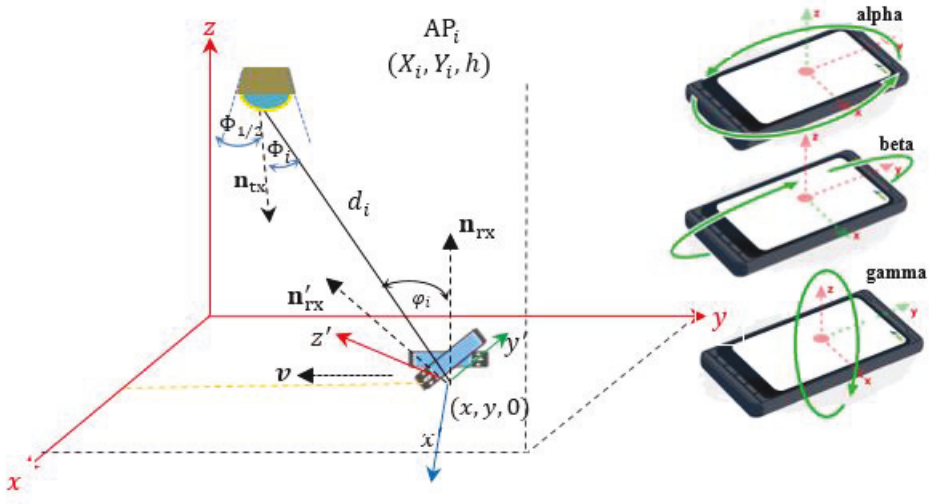

Figure 4.2 : Modelling of the receiver's orientation based on rotations around three axes [3].

The angle α describes rotation around the z-axis, and because UE is assumed to be always on the ground plane, the angle α takes a value between 0^o and 360^o . The angles β and γ (both range from -90^o to 90^o) are the rotation angles around the x- and y-axis respectively. The range of angles is chosen so as to ensure that the UE is able to communicate with at least one AP [36]. These values are similar to the angles used in [5].

Another parameter is the distance vector between a UE (x, y, z) and every AP_i (X_i, Y_i, Z_i) and the magnitude of this vector is called the Euclidean distance between AP_i and the UE and it is calculated as follows [36]:

$$d_i = ||\boldsymbol{d_i}|| = \sqrt{(X_i - x)^2 + (Y_i - y)^2 + (Z_i - z)^2} \tag{4.6}$$

There are two angles of interest between the UE and AP. They are ϕ_i and φ_i which

are the angles of radiance with respect to the z-axis (vertical) on the transmitter plane and the receiver plane for AP_i, respectively [36]. The angles ϕ_i and φ_i are described mathematically in the following equations using the rules of geometry:

$$cos\phi_i = d_i.n_{tx}/||d_i|| \tag{4.7}$$

$$cos\varphi_i = -d_i.n_{rx}/||d_i|| \tag{4.8}$$

where

- n_{rx} and n_{tx}: the normal vectors of the receiver and transmitter planes respectively
- || || and .: the Euclidean norm operators and inner product respectively.

The optical concentrator gain of the receiver is given by

$$g(\varphi_i) = \begin{cases} \frac{m^2}{sin(\varphi_c)^2} & 0 \leq \varphi_i \leq \varphi_c \\ 0 & \varphi_i > \varphi_c \end{cases} \tag{4.9}$$

where

- m is the refractive index

4.3 Simulation Model

In this research, UE moves within the room at a constant speed in a rectangular spiral pattern. The rectangular spiral pattern is chosen due to its full coverage around the whole area in order to have a proper evaluation. UE starts moving from the point (-5,-5) in an easterly direction until reaching the edge of the simulation area. Then this path is repeated in the northerly, westerly and southerly directions.

After completing one round, the UE moves one meter inward and this cycle is repeated until the UE reaches the center of the room. The numbers on the sprial pattern represent the moving time in seconds and it takes 1200 seconds to complete this spiral path [36].

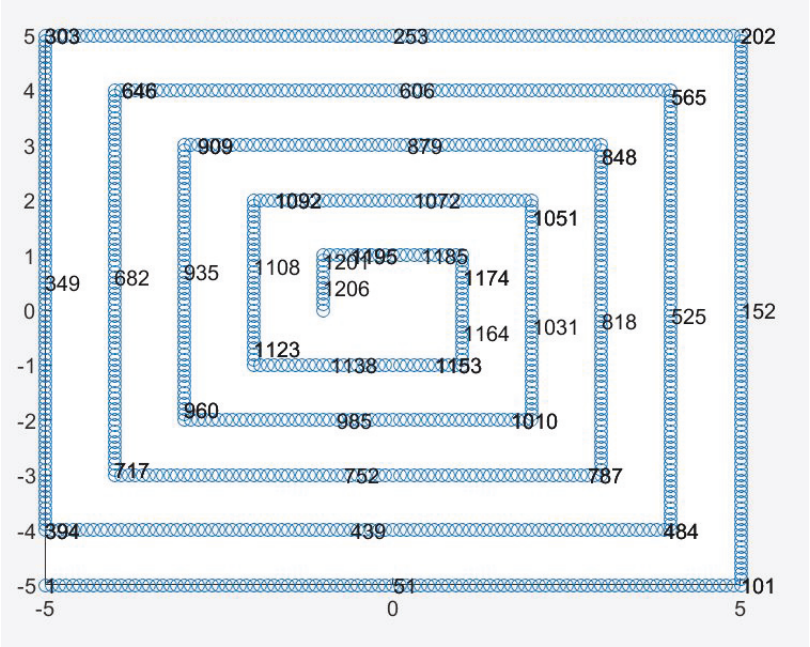

Figure 4.3 : UE mobility modelling [36, 38].

4.4 Single Beam LEDs Model

4.4.1 Single Beam LEDs Li-Fi System Configuration

Fig. 4.4 shows the overview of the indoor optical system which contains four LED transmitters (or Access Point - AP) in the center of the four quarters of the room's ceiling, and a UE device plays the receiver role on the floor [36]. In this research, the Way Point Model [7] was applied for user movement within a square area of dimensions of b x b (m^2) [36].

The assumptions in this single beam LED model are [36]:

i. LED transmitters follow "the Lambertian emission patterns and operate within

the linear dynamic range of the current-to-power characteristic curve to reduce effects of nonlinear distortion" [2].

ii. These LED transmitters emit light vertically downwards.

iii. UE can be rotated in any direction.

iv. All LED transmitters have the same transmit power, and one unique AP is chosen for serving the UE depending on its orientation and location.

v. Reflection on the wall, ceiling, and floor surfaces will not be considered.

vi. Line-of-sight (LOS) communication channel is considered in this research only.

vii. UE device is always on the ground plane of the network area.

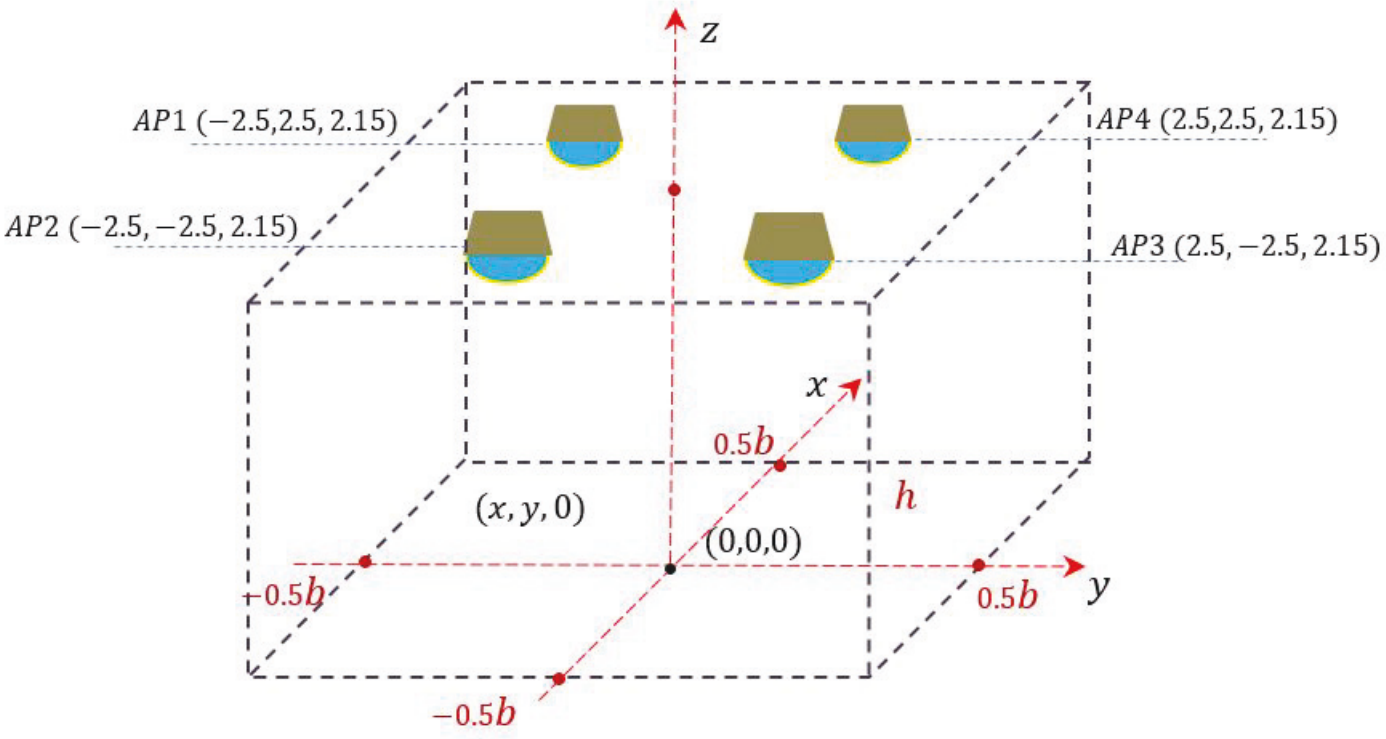

Figure 4.4 : The simulated optical network system [36].

4.4.2 Single Beam LEDs Li-Fi System Parameters

The parameters that have been used in this research are given in the following table:

Table 4.1 : Simulation single beam LED set up [36].

Name of Parameters	**Value**
Network space (L x W x H)	10m x 10m x 2.15m
Number of APs	4
Location of AP1	(-2.5,-2.5, 2.15)
Location of AP2	(-2.5,2.5, 2.15)
Location of AP3	(2.5,-2.5, 2.15)
Location of AP4	(2.5,2.5, 2.15)
LED half-intensity angle $\phi_{1/2}$	60^o
Receiver FOV ψ_c	90^o
Optical filter gain T_s	1
Effective photodetector area A	1×10^{-4}
Refractive index m	1

4.4.3 Single Beam LEDs Li-Fi System Flowchart

This modelling is conducted based on Fig. 4.4.3 :

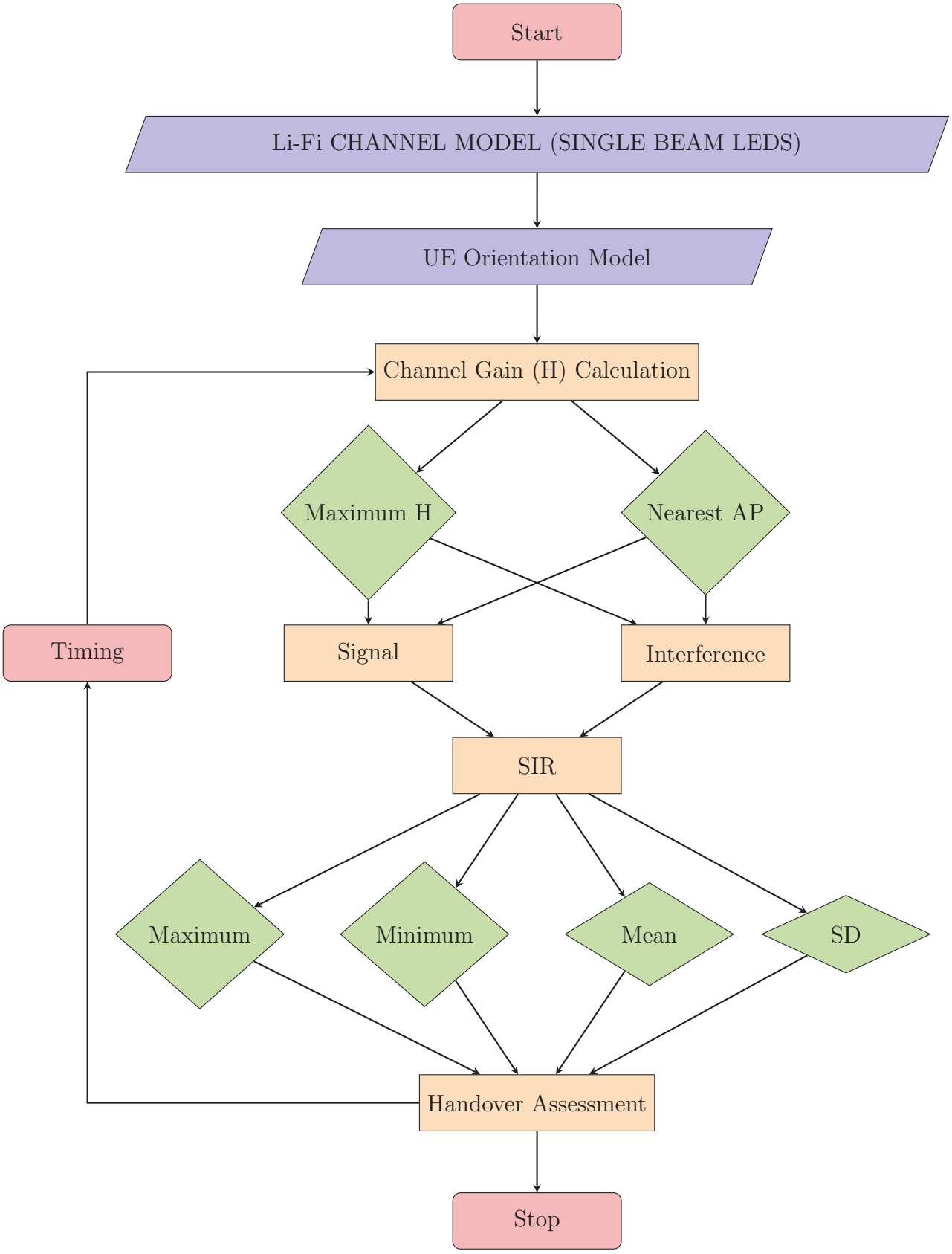

Figure 4.5 : Single Beam LEDs Li-Fi System Flowchart

4.5 Multiple Beams LEDs Model

4.5.1 Multiple Beams LEDs Li-Fi System Configuration

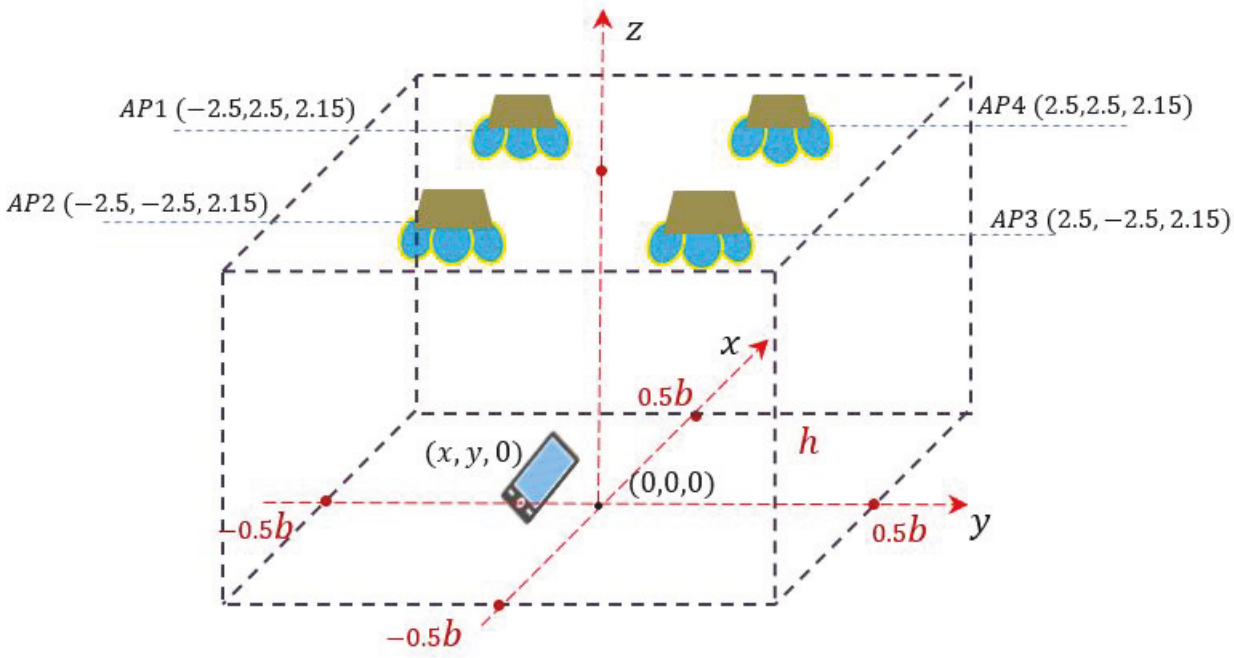

Figure 4.6 : Multiple beams LED optical network system [38].

The overview of the indoor multiple beams LED system is shown in the Fig. 4.6 which contains four multiple beams LED transmitters in the four quarters of the room's ceiling, and a UE device plays the receiver role on the floor. Multiple beams LEDs are considered as the multiple beams Access Point (AP). The Way Point Model [7] was applied in this research for user movement within a square area of dimensions of b x b (m^2).

The multiple beams LED is described in the following figure (Fig. 4.7) where four beams from one LED have been configured. The vertical inclination angle between each beam and vertical axis are equal.

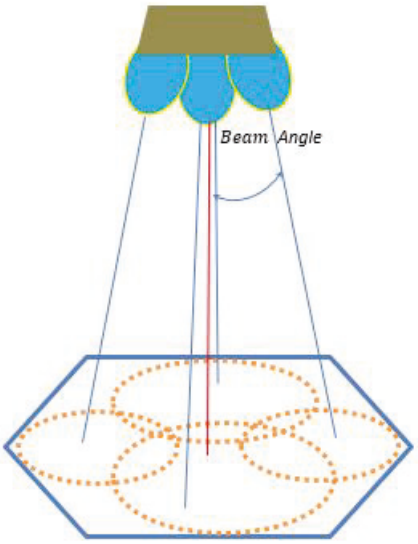

Figure 4.7 : The layout of the optical scenario with an angle diversity optical transmitter [38].

The layout from the top is shown in Fig. 4.8. Each beam has its own coverage area and maybe overlapped with the coverage area of other beams depending on beam width and angle.

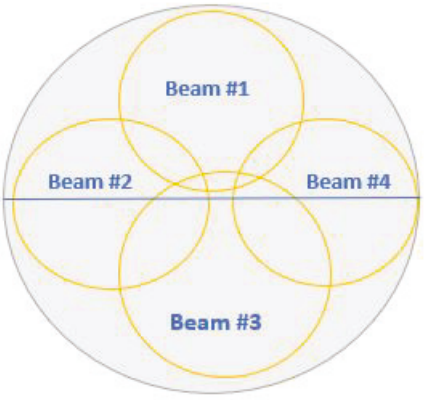

Figure 4.8 : The layout of a 4-element angle diversity transmitter [38].

4.5.2 Multiple Beams LEDs Li-Fi System Parameters

The parameters that are used in this research are given in Table 4.2

Table 4.2 : Simulation parameters in multiple beams environment [38].

Name of Parameters	**Value**
Network area (L x W x H)	10m x 10m x 2.15 m
Number of APs	4
Number of beams per LED	4
AP1 location	(-2.5, 2.5, 2.15)
AP2 location	(-2.5, -2.5, 2.15)
AP3 location	(2.5, -2.5, 2.15)
AP4 location	(2.5, 2.5, 2.15)
LED half-intensity angle $\phi_{1/2}$	60^o
Receiver FOV ψ_c	90^o
Optical filter gain T_s	1
Effective photodetector area A	$1{\times}10^{-4}$
Refractive index m	1

The assumptions in this multiple beams LED model are:

i. All LED transmitters emit light in four directions of four beams.

ii. The rotation of UE device can be random in three directions x, y and z.

iii. All beams emit the same power and only one beam is considered for serving the UE based on its rotated angle and location.

iv. Reflection on any surface: wall, ceiling & floor will not be considered.

v. Only line-of-sight (LOS) channel are considered.

vi. UE device is always held by a person at one meter height from the floor in the simulated area.

4.5.3 Multiple Beams LEDs Li-Fi System Flowchart

This modelling is conducted based on the following flowchart:

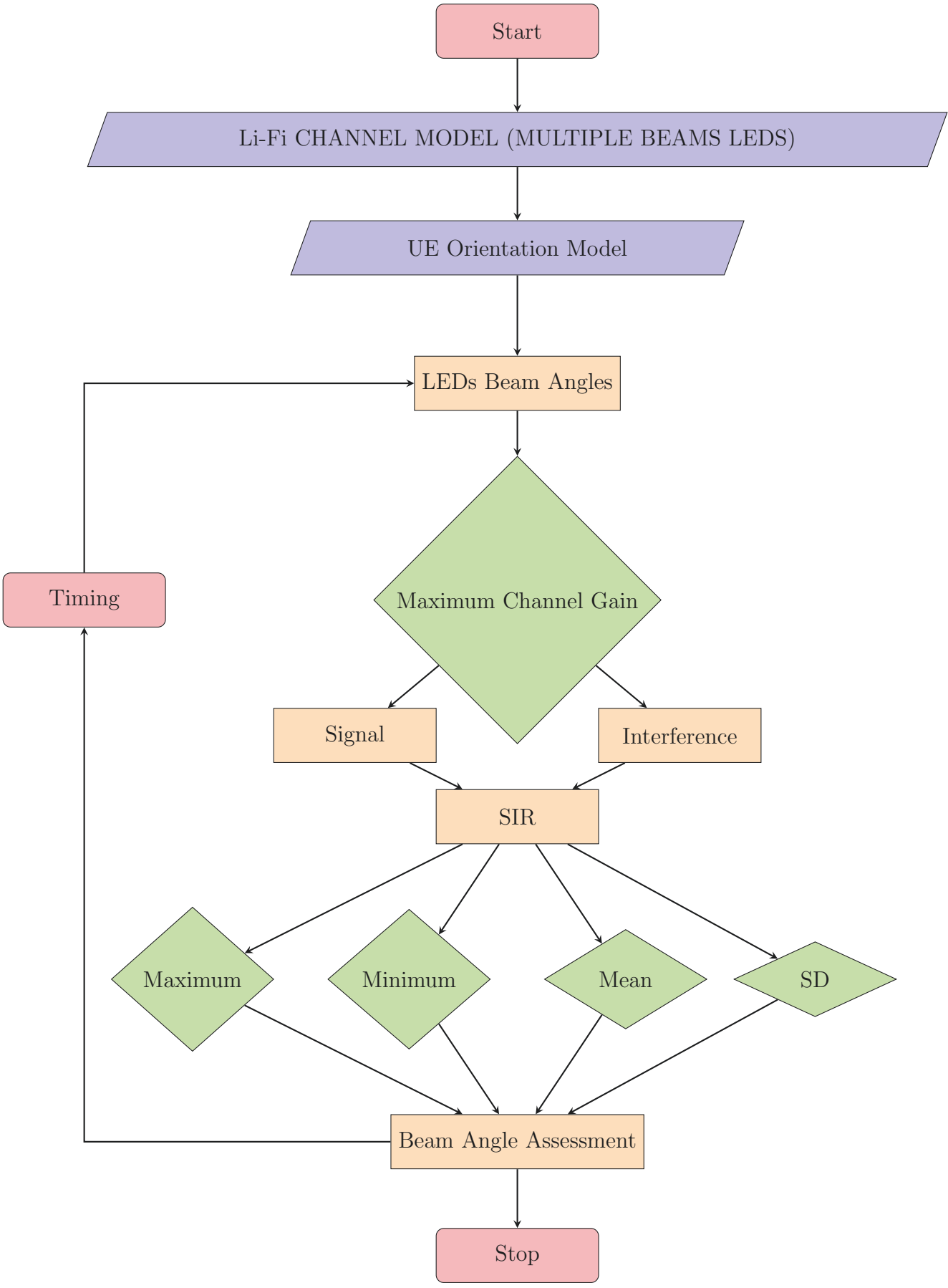

Figure 4.9 : Multiple Beams LEDs Li-Fi System Flowchart

4.6 Conclusion

In this chapter, the modelling and simulation of the research are presented. The Li-Fi channel is described, including the Lambertian irradiance pattern and channel gain formulas. Thereafter, the geometric orientation model is presented with the modelling of receiver orientation based on rotations around three axes. The Euclidean distance and optical concentrator of the receiver are also given in this chapter. In the next sections, the simulation model of spiral path is presented followed by the single beam and multiple beams LEDs models. In these two parts, the system configuration and simulation parameters are listed.

Chapter 5

Performance Analysis of Single Beam LEDs Model

This chapter contains the results of performance analysis of single beam LEDs. The next chapter extends the work in this chapter to a multi beam Li-Fi network.

5.1 Channel Gain Assessment

When a UE is moving along the rectangular spiral path (see Fig. 4.3), with fixed values of α, β and γ for each cycle, the channel gain values vary as shown in the following figure [36].

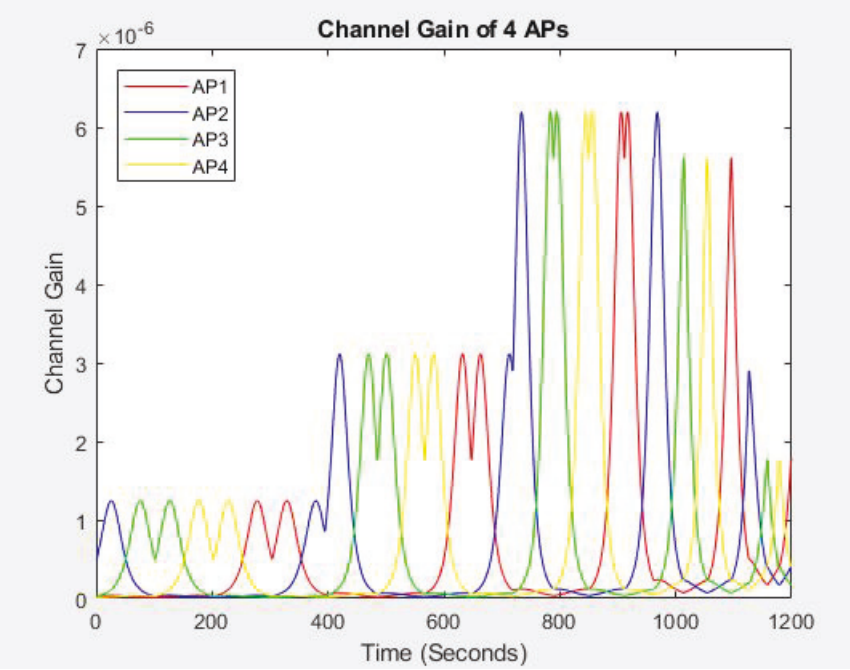

Figure 5.1 : Channel gain of four APs when $\alpha = 0$, $\beta = 0$ and $\gamma = 0$ [36].

Fig. 5.1 shows the channel gain observed by the UE as it moves in the spiral path facing the default direction ($\alpha = 0$, $\beta = 0$ and $\gamma = 0$). Each colour represents channel gain from each of the four APs in the room. Initially, when the UE is moving on the perimeter of the rectangle in an anticlockwise direction, the UE is furthest away from the APs and hence the channel gain observed are small from all APs. At time t = 0, the UE is at the location (-5, -5) (Fig. 4.3) and it is closest to AP2 at (-2.5, -2.5) (Fig. 4.3) and hence the signal from AP2 (shown in blue) is the strongest signal. Thereafter, between times t = 51 seconds and t = 100 seconds, the UE is closest to AP3 at (2.5, -2.5) and hence the signal from AP3 shown in green has the strongest channel gain. At time t = 400 seconds, the UE has almost completed a full rotation and returned close to the start point and the signal from AP2 shown in blue is the strongest signal. The channel gain at t = 400 seconds is higher than at t = 0 because the UE is now closer to AP1 [36].

From 0 to 1200 seconds, there are five different patterns because there are five anticlockwise cycles in that spiral path. On each cycle, the UE has nearly equal channel gain values from each AP. When UE is on $1^{st}, 2^{nd}, 3^{rd}$ and 5^{th} cycle, its channel gain is smaller because its distance to the APs is furthest. In contrast, in the 4^{th} cycle, its channel gain is highest due to the nearest distance between UE and APs.

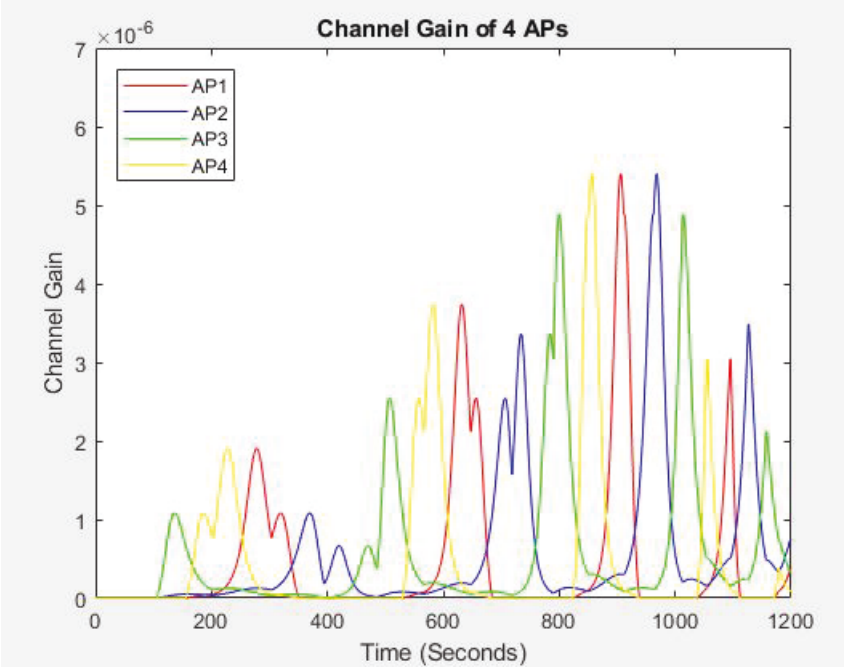

Figure 5.2 : Channel gain of four APs when $\alpha = 0$, $\beta = 45^0$ and $\gamma = 0^0$ [36].

After changing values of β to 45^0 (Fig. 5.2), the four APs' channel gain values reduce slightly. Moreover, the values are minimal after the first 100 seconds which is close to zero. Similarly, the channel gain values are small in the outer rounds and become larger when getting closer to the room center [36].

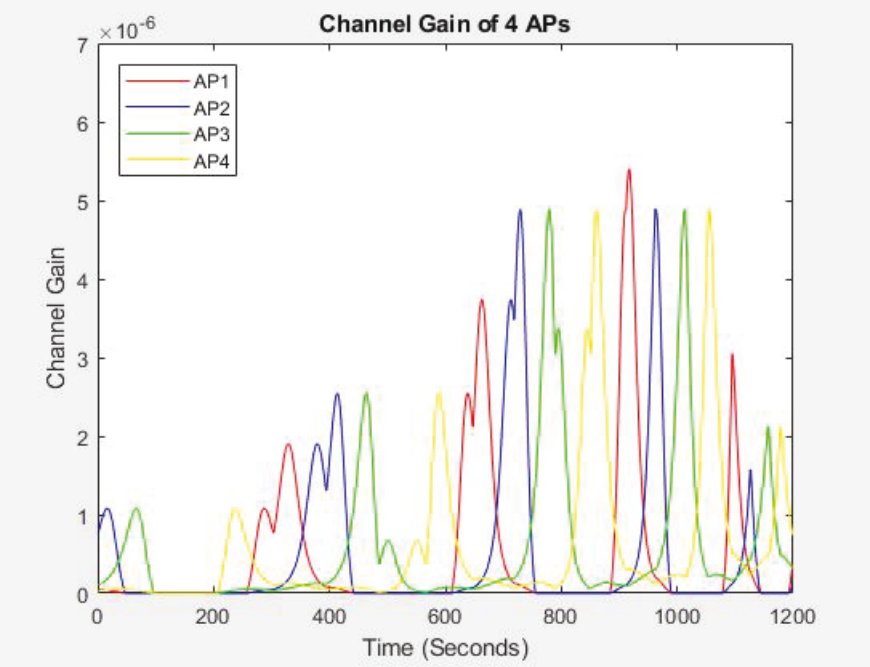

Figure 5.3 : Channel gain of four APs when $\alpha = 0$, $\beta = 0$ and $\gamma = 45^0$ [36].

Repeating the same test with γ of 45^0 (Fig. 5.3), the channel gains are almost matching the values in Fig. 5.2, but the minimal values are from 100 to 200 seconds. The channel gain values have similar patterns - small in the outer paths and larger when getting closer to the APs in the room center.

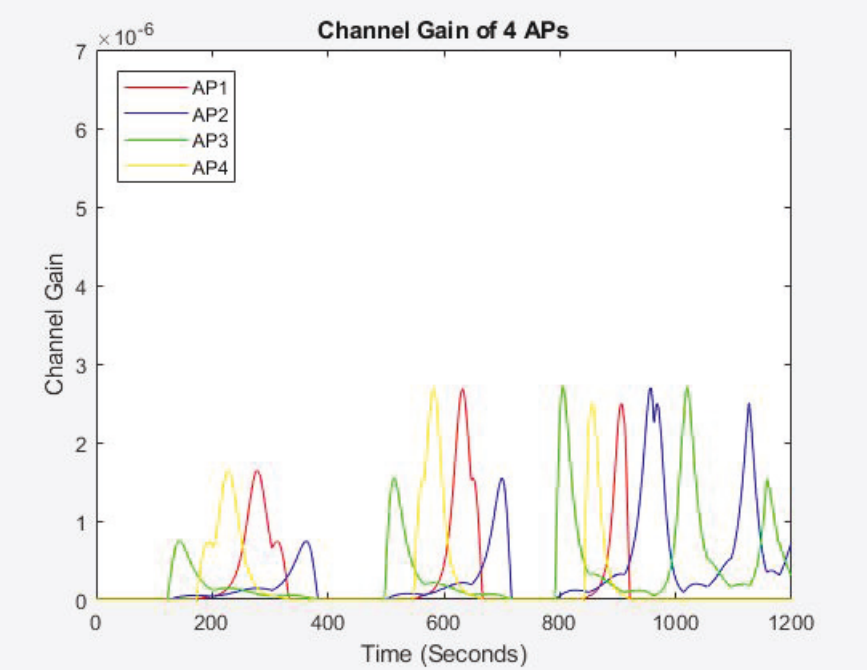

Figure 5.4 : Channel gain of four APs when $\alpha = 0$, $\beta = 80^0$ and $\gamma = 0$ [36].

In Fig. 5.4, there is a symmetry between channel gain of AP4 and AP1, AP3 and AP2 within three time frames when the values of β are changed to 80^0. They are increased when UE moves to the room center where it comes closer to the light source.

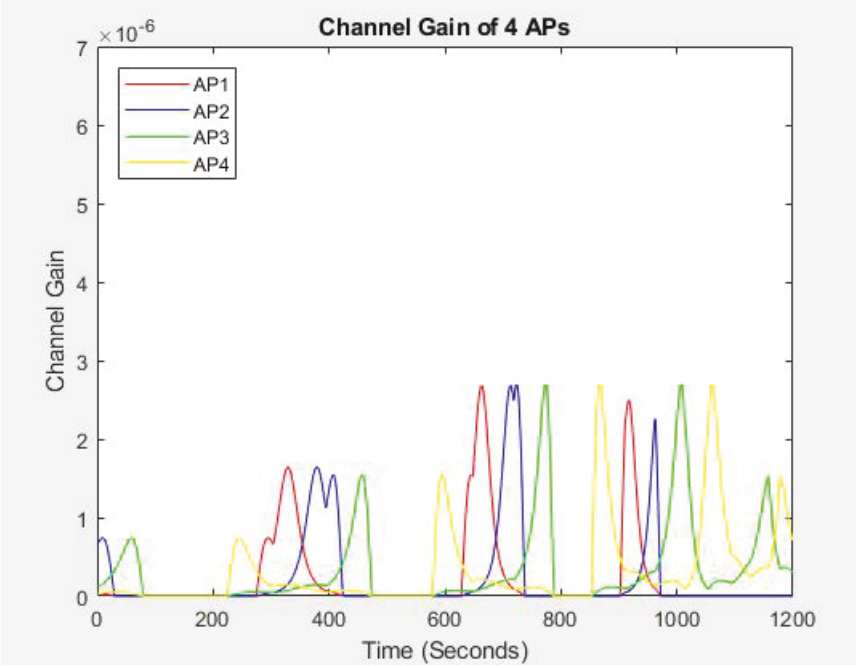

Figure 5.5 : Channel gain of four APs when $\alpha = 0$, $\beta = 0$ and $\gamma = 80^0$ [36].

There is a similarity between Fig. 5.4 and Fig. 5.5 because there is symmetry for measurements in one cycle. However, signal values in Fig. 5.5 are advanced by 50 seconds compared to Fig. 5.4 due to the difference between values of rotating angles about x- and y-axis.

5.2 Maximum-channel-gain-based Handover Decision

In order to find the serving AP among four APs on the ceiling, the maximum values of channel gain are selected so that the received signal is continuous while the UE moves around the network area. These values are plotted in the following figure [36]:

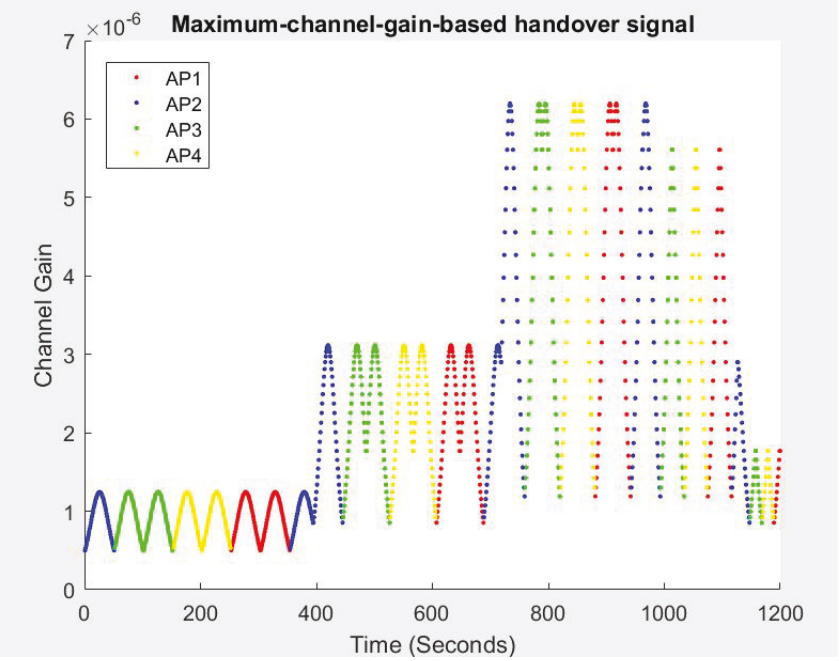

Figure 5.6 : Maximum-channel-gain-based signal when $\alpha = 0$, $\beta = 0$ and $\gamma = 0$ [36].

When the handover algorithm is choosing the maximum value of channel gain (Fig. 5.6), the shape of UE's received signal is similar to the maximum values in Fig. 5.1. Firstly, UE is served by AP2 (blue line) and then by AP3 (green line), AP4 (yellow line) and AP1 (red line), respectively. At the time of 400 seconds, this value increases to more than double the previous value as the UE is now in another cycle inside the room. Then it continues the remaining path at that level until a time of 750 seconds [36].

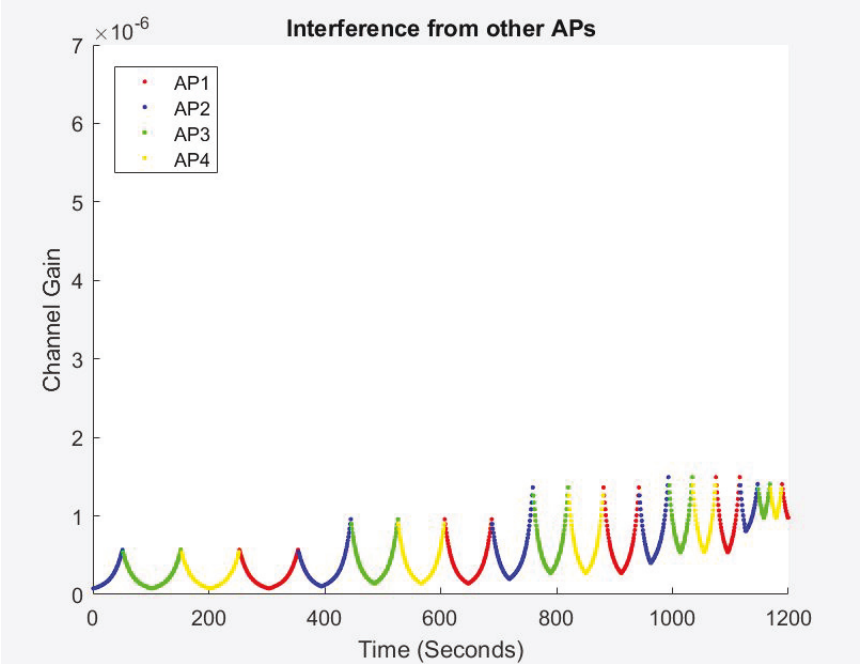

Figure 5.7 : Maximum-channel-gain-based interference when $\alpha = 0$, $\beta = 0$ and $\gamma = 0$ [36].

If the UE is served by one AP which is considered as desired signal, then the other three APs would be considered as interference. Fig. 5.7 shows the total interference of the other three APs when UE is served by any AP. When UE is served by AP2, the blue graph shows the total interference of all AP1, AP3 and AP4. And then when it is served by AP3, the channel gain from AP1, AP2 and AP4 will be considered as the interference. In this case, the communication is possible during 94.71% of the whole path (Table 5.2). However, the maximum value of SIR is 13.13 and the average value is 8.4 which is suitable for light communication channel (Table 5.1) [36].

Table 5.1 : Channel gain statistics of maximum-channel-gain-based handover decision when $\alpha = 0$, $\beta = 0$ and $\gamma = 0$ [36].

Maximum-channel-gain-based handover	Maximum	Minimum	Mean	Standard deviation
Gain value (10^{-6})	6.20	0.50	1.71	1.57
Interference value (10^{-6})	1.49	0.08	0.38	0.35
SIR (dB)	13.13	-2.16	8.4	7.11

From Table 5.2, we could see that communication is possible for 94.71% of the time and this percentage reduces approximately 25% when requirements of SIR are 3dB (77.93%) and 7dB (56.20%). There is only 23.47% of the time where SIR is larger than 10dB.

Table 5.2 : The overall system performance of maximum-channel-gain-based handover decision when $\alpha = 0$, $\beta = 0$ and $\gamma = 0$ [36].

	SIR>0 dB	SIR>3dB	SIR>7 dB	SIR>10dB
Percentage of time (%)	94.71	77.93	56.20	23.47

Fig. 5.8 shows the received signal of UE when the handover decision is based on the maximum channel gain between four APs at one time. The signal is zero at the period from 0 to 100 seconds and then it was chosen among four APs' signals to find UE's signal.

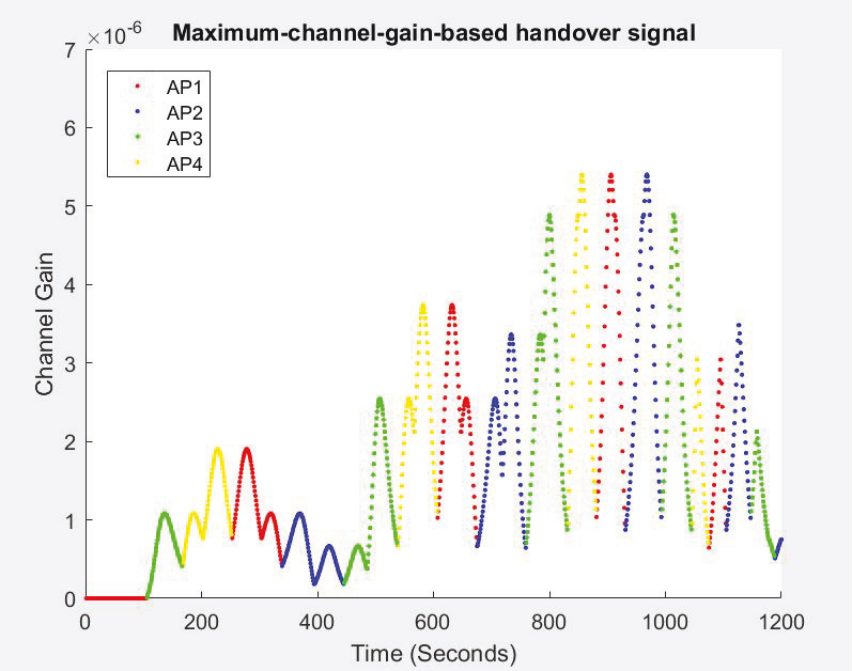

Figure 5.8 : Maximum-channel-gain-based signal when $\alpha = 0$, $\beta = 45^0$ and $\gamma = 0$ [36].

The interference in Fig. 5.9 is quite small when compared to the received signal so it does not have much effect on the communication channel when UE is tipping at 45^0 around x-axis. For 8.8% of the time, there is no communication during this path. Although the maximum value of SIR is quite high (51.22) (Table 5.3) when compared to the previous case but the average value is lower (5.21).

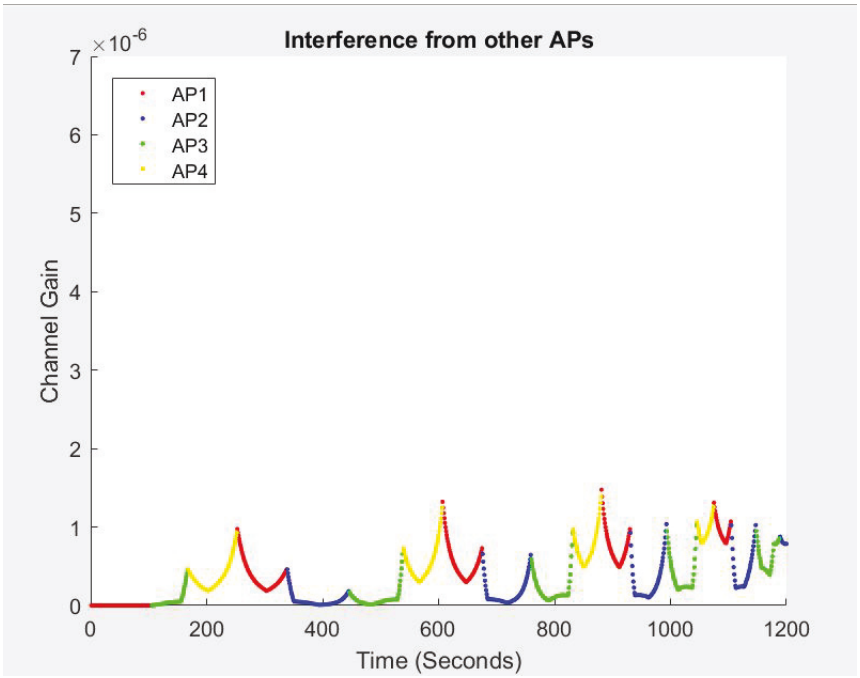

Figure 5.9 : Maximum-channel-gain-based interference when $\alpha = 0$, $\beta = 45^0$ and $\gamma = 0$ [36].

Table 5.3 : Channel gain statistics of maximum-channel-gain-based handover decision when $\alpha = 0$, $\beta = 45^0$ and $\gamma = 0$ [36].

Maximum-channel-gain-based handover	Maximum	Minimum	Mean	Standard deviation
Gain value (10^{-6})	5.4	0	1.31	1.32
Interference value (10^{-6})	1.47	0	0.25	0.32
SIR (dB)	51.22	0	5.21	12.99

Table 5.4 : The overall system performance of maximum-channel-gain-based handover $\alpha = 0$, $\beta = 45^0$ and $\gamma = 0$ [36].

	SIR>0 dB	SIR>3dB	SIR>7 dB	SIR>10dB
Percentage of time (%)	86.02	74.44	51.12	32.42

When the UE is inclined at 45^0 along y axis (Fig. 5.10), the signal is minimal from 100 to 200 seconds. The received signal value is similar to Fig. 5.8 and the maximum and minimum values remain the same (5.4 x 10^{-6} and 0) which are shown Table 5.3 and 5.4.

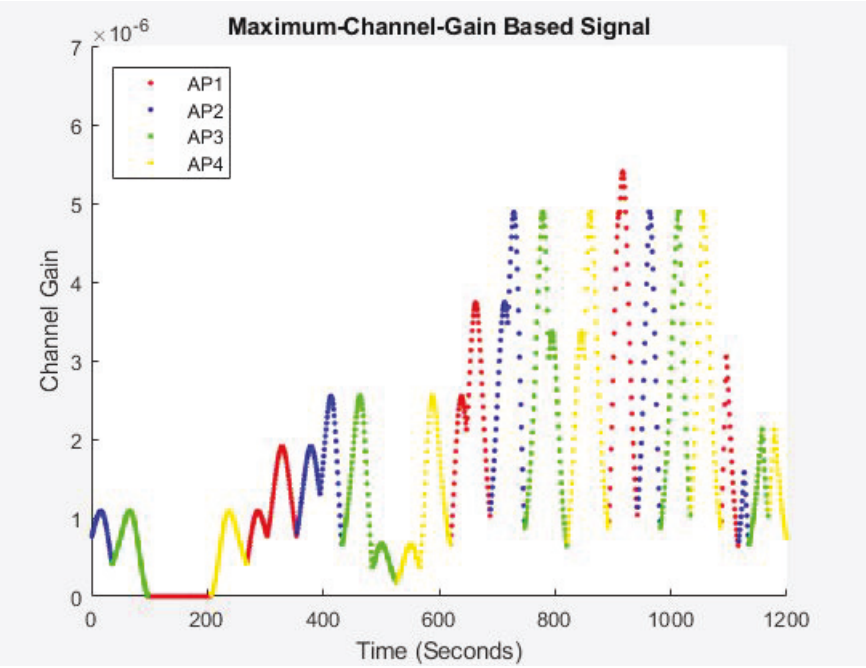

Figure 5.10 : Maximum-channel-gain-based signal when $\alpha = 0$, $\beta = 0$ and $\gamma = 45^0$ [36].

The interference signal from 100 to 200 seconds is quite small when compared to the receiving signal (Table 5.5). There is no communication for 9.14% of the time

during this test. Similarly, the maximum, minimum and mean values of SIR remains when UE's rotation is changed from around x-axis to y-axis.

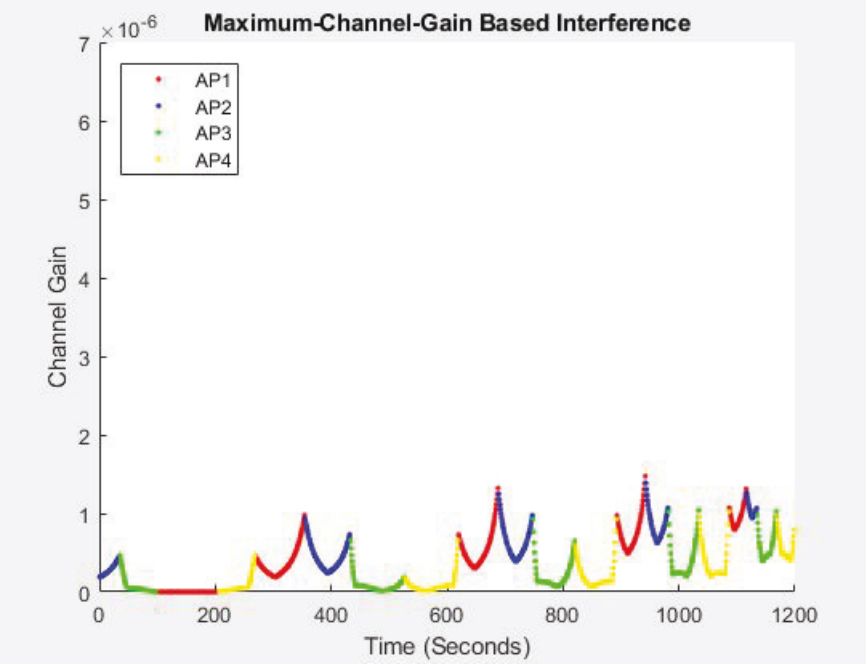

Figure 5.11 : Maximum-channel-gain-based interference when $\alpha = 0$, $\beta = 0$ and $\gamma = 45^0$ [36].

Table 5.5 : Channel gain statistics of maximum-channel-gain-based handover decision when $\alpha = 0$, $\beta = 0$ and $\gamma = 45^0$ [36].

Maximum-channel-gain-based handover	Maximum	Minimum	Mean	Standard deviation
Gain value (10^{-6})	5.4	0	1.32	1.31
Interference value (10^{-6})	1.47	0	0.249	0.321
SIR (dB)	51.22	0	5.27	12.98

When the angles of β and γ increase to 80^0, the difference in level could be seen in

Fig. 5.12 to 5.15. There was the same pattern of signal and interference between two cases: $\beta = 80^0$, $\gamma = 0$ and $\beta = 0$, $\gamma = 80^0$ ($\alpha = 0$ for both cases). However, the values in the second case ($\alpha = 0$, $\beta = 0$ and $\gamma = 80^0$) have moved 70 seconds forward compared to the first case ($\alpha = 0$, $\beta = 80^0$ and $\gamma = 0$).

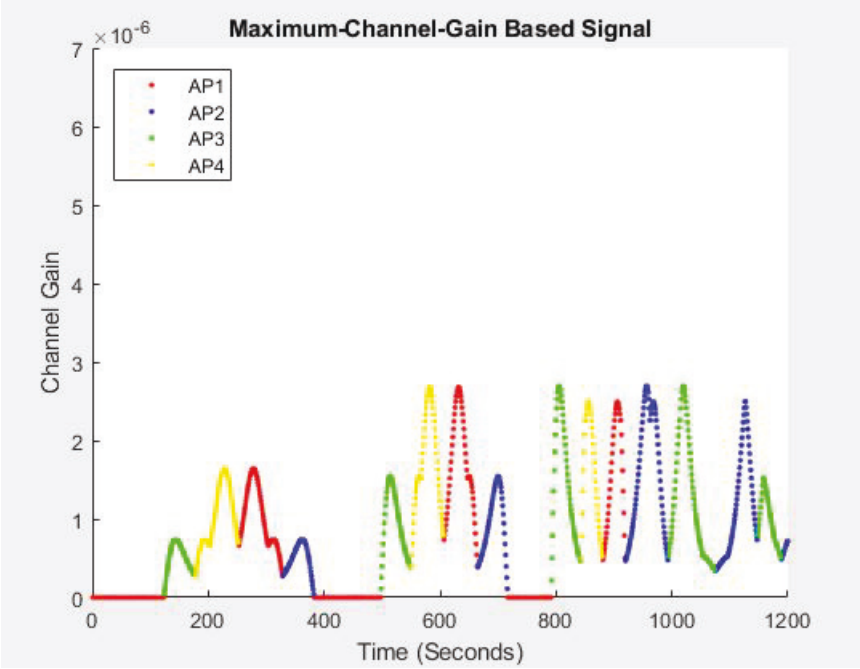

Figure 5.12 : Maximum-channel-gain-based signal when $\alpha = 0$, $\beta = 80^0$ and $\gamma = 0$ [36].

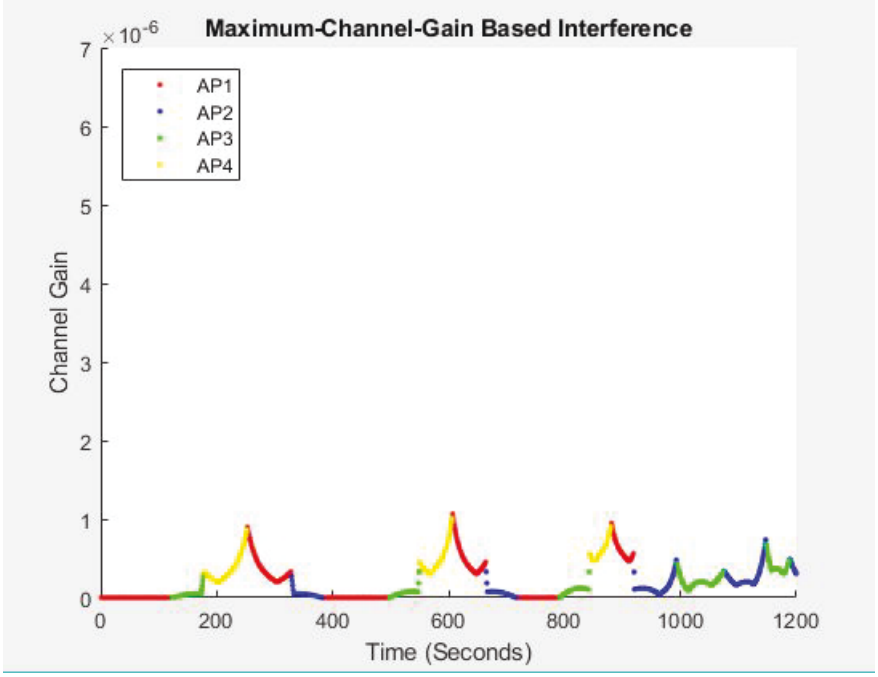

Figure 5.13 : Maximum-channel-gain-based interference when $\alpha = 0$, $\beta = 80^0$ and $\gamma = 0$ [36].

Table 5.6 : Channel gain statistics of maximum-channel-gain-based handover decision when $\alpha = 0$, $\beta = 80^0$ and $\gamma = 0$ [36].

Maximum-channel-gain-based handover	Maximum	Minimum	Mean	Standard deviation
Gain value (10^{-6})	2.7	0	0.715	0.078
Interference value (10^{-6})	1.06	0	0.012	0.022
SIR (dB)	51.22	0	3.32	11.08

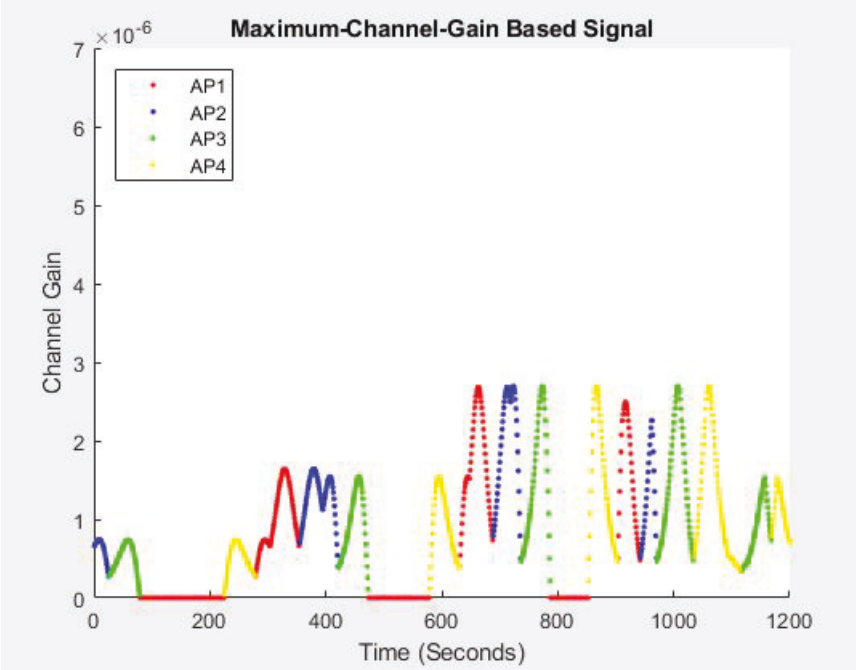

Figure 5.14 : Maximum-channel-gain-based signal when $\alpha = 0$, $\beta = 0$ and $\gamma = 80^0$ [36].

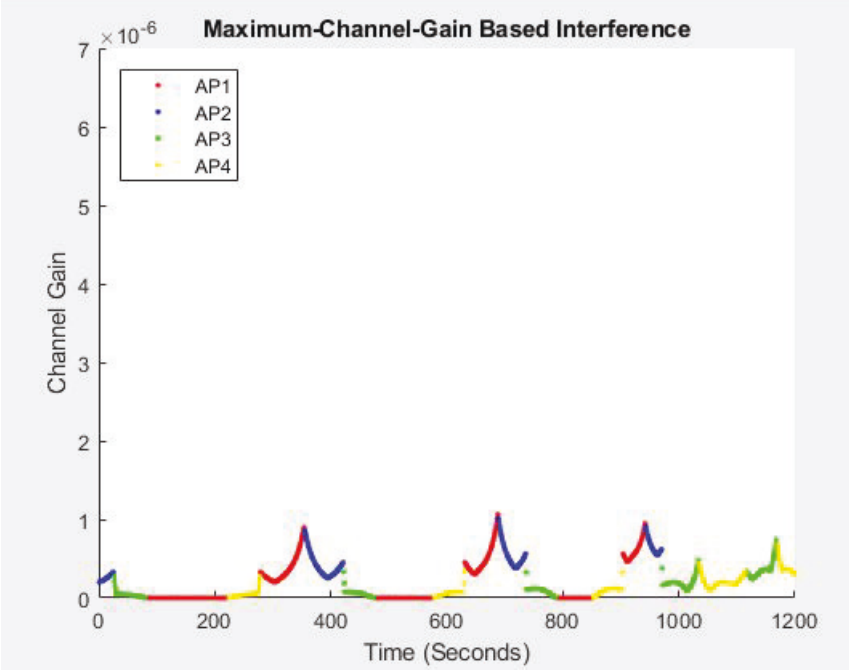

Figure 5.15 : Maximum-channel-gain-based interference when $\alpha = 0$, $\beta = 0$ and $\gamma = 80^0$ [36].

In both cases ($\alpha = 0$, $\beta = 80$ and $\gamma = 0$ and $\alpha = 0$, $\beta = 0$ and $\gamma = 80^0$), for 26% of the time there is no communication during this test. Although the maximum value is quite high (51.22) but the mean value is quite low (3.32), and hence there are two cases considered as the worst case scenario when UE is tipping 80^0 around x and y axis.

Table 5.7 : Channel gain statistics of maximum-channel-gain-based handover decision when $\alpha = 0$, $\beta = 0$ and $\gamma = 80^0$ [36].

Maximum-channel-gain-based handover	Maximum	Minimum	Mean	Standard deviation
Gain value (10^{-6})	2.7	0	0.717	0.078
Interference value (10^{-6})	1.06	0	0.016	0.0223
SIR (dB)	51.22	0	3.32	11.32

In summary, Fig. 5.6 and 5.7 show the received signal and interference based on the maximum channel gain when UE is in a normal direction. It can be seen that the Signal to Interference ratio (SIR) is quite low in the first quarter of the path. However, this ratio was increased gradually in the remainder of the UE path. When the angles (β and γ) are changed to 45^0, both signal and interference values were small (Fig. 5.8 to 5.11) due to different paths between APs and photodetector. However, when these two angles are changed to 80^0, the SIR was quite high as shown in the Fig. 5.12 to 5.15.

The selection of maximum channel gain values for indoor Li-Fi network was conducted in this research. When the user moved closer to the center of the room where the high values of channel gain exist, the handover process performs better due to the large density of transmitted signals from four LEDs. The receiver rotation has a

significant impact on the channel gain values when UE is moving around the network area.

5.3 Nearest-AP-based Handover Decision

In order to find the serving AP among four APs on the ceiling, the nearest APs are selected to serve UE while the UE moves around the network area. These values are plotted in the following figure [36]:

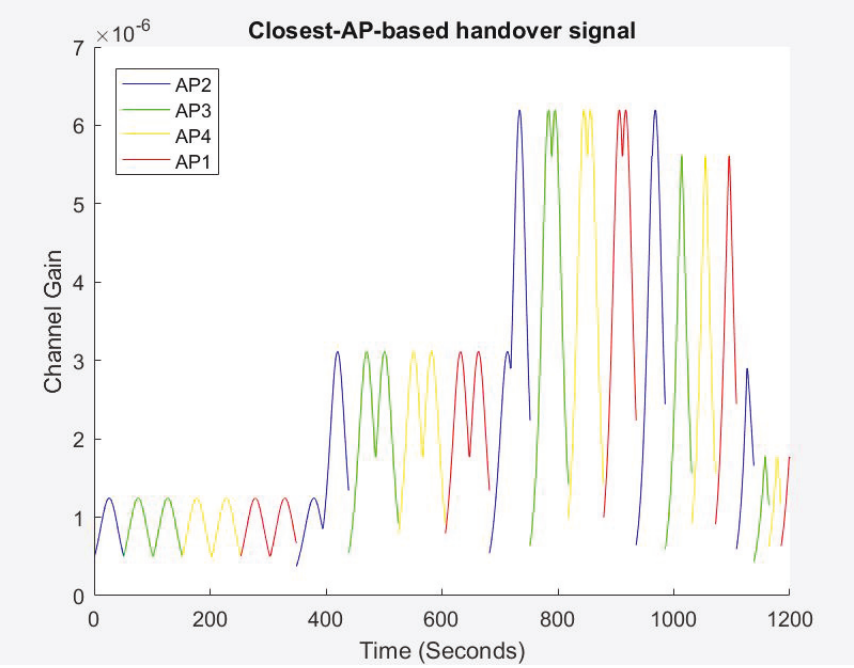

Figure 5.16 : Nearest-AP-based signal when $\alpha = 0$, $\beta = 0$ and $\gamma = 0$ [36].

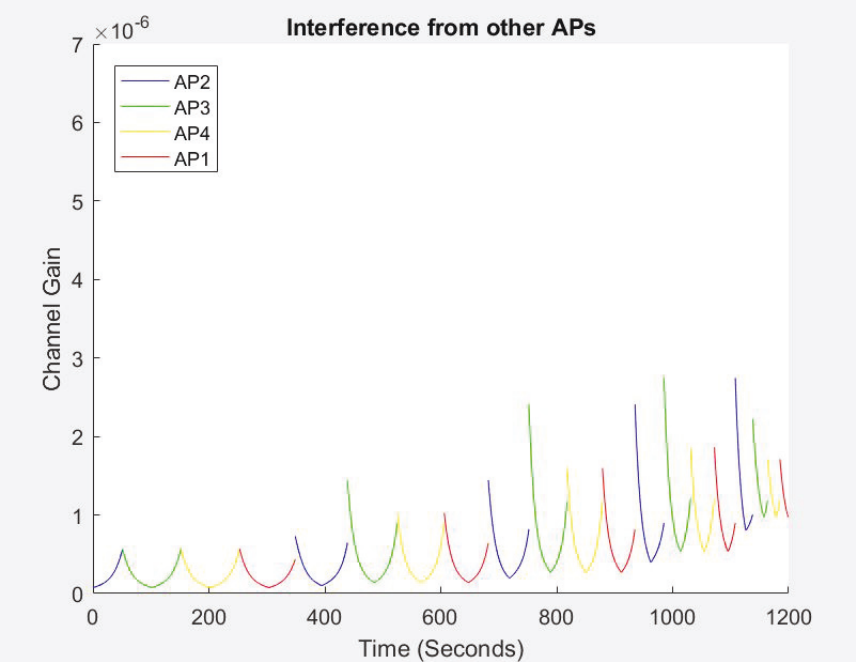

Figure 5.17 : Nearest-AP-based interference when $\alpha = 0$, $\beta = 0$ and $\gamma = 0$ [36].

When $\alpha = 0$, $\beta = 0$ and $\gamma = 0$, the UE's signal pattern looks like the patterns of handover algorithms by choosing the maximum channel gain values in Fig. 5.6. However, there is a discontinuity here as it is chosen regardless of maximum channel gain value. There is a gap in channel gain at 350 sec when UE-serving AP is transferred from AP1 to AP2. In this case, the communication channel remains during 47.23% of the whole path (Table 5.9). The maximum and minimum values of SIR are 13.12 dB and -17.2 dB respectively but the mean value is quite low, only -1.12 dB (Table 5.8) [36].

Table 5.8 : Channel gain statistics of nearest-AP-based handover decision when $\alpha = 0$, $\beta = 0$ and $\gamma = 0$ [36].

Nearest-AP-based handover	Maximum	Minimum	Mean	Standard deviation
Gain value (10^{-6})	6.2	0.014	0.135	1.21
Interference value (10^{-6})	2.8	0.076	1.38	1.65
SIR (dB)	13.12	-17.2	-1.12	6.98

Table 5.9 : The overall system performance when $\alpha = 0$, $\beta = 0$ and $\gamma = 0$ [36].

	SIR>0 dB	SIR>3dB	SIR>7 dB	SIR>10dB
Percentage of time (%)	47.23	39.04	28.45	11.58

When the handover algorithm is based on the minimum distance between UE and APs and the $\beta = 45^0$ (Fig. 5.18), there would be a gap between received signal value while UE is moving. This is because the algorithm only chooses the channel gain of nearest AP without considering whether the channel gain is maximised or not. For 82.05% of time there is no communication during this path as this is not considered as a good channel (Table 5.11). Additionally, the maximum value of SIR is only 10.13 and the minimum and mean values are 0. To conclude, when UE is tipping 45^0 around x axis and the handover algorithms based on the nearest APs, the signal is not good at all [36].

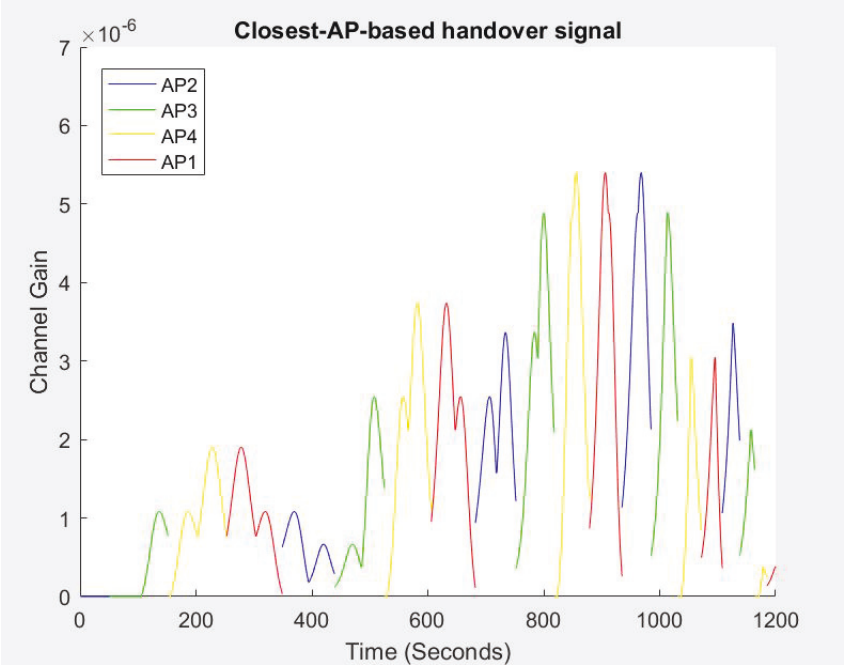

Figure 5.18 : Nearest-AP-based signal when $\alpha = 0$, $\beta = 45^0$ and $\gamma = 0$ [36].

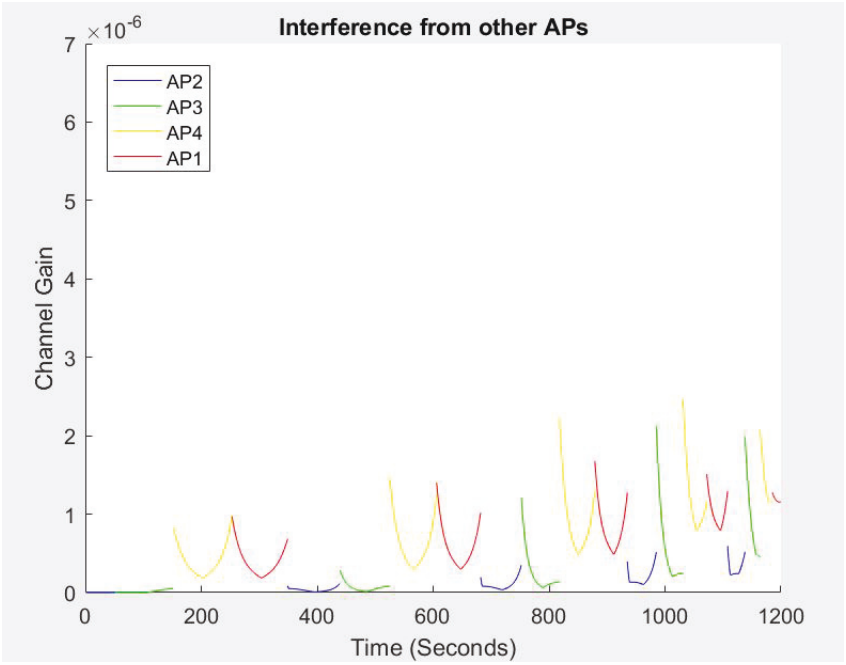

Figure 5.19 : Nearest-AP-based interference when $\alpha = 0$, $\beta = 45^0$ and $\gamma = 0$ [36].

Table 5.10 : Channel gain statistics of nearest-AP-based handover decision when $\alpha = 0$, $\beta = 45^0$ and $\gamma = 0$ [36].

Nearest-AP-based handover	Maximum	Minimum	Mean	Standard deviation
Gain value (10^{-6})	5.4	0	0	0.974
Interference value (10^{-6})	2.3	0	1.18	1.34
SIR (dB)	10.13	0	0	2.05

Table 5.11 : Overall system performance when $\alpha = 0$, $\beta = 45^0$ and $\gamma = 0$ [36].

	SIR>0 dB	SIR>3dB	SIR>7 dB	SIR>10dB
Percentage of time (%)	17.95	14.64	7.03	0.25

Similarly, when γ is changed to 45^0, the channel gains are minimal from 100 to 250 seconds (Fig. 5.20). However, the interference values become zero in many instants during this path. In this case, for 9.39% of the time there is no communication and the maximum value of SIR has increased up to 51.22 (Table 5.12). However, the mean value of SIR is only 0.07 with a SD of 10.88. When UE rotates around the x and y axis and the minimum-distance-based handover algorithm applied, the values are not the same like the maximum channel gain based handover algorithm [36].

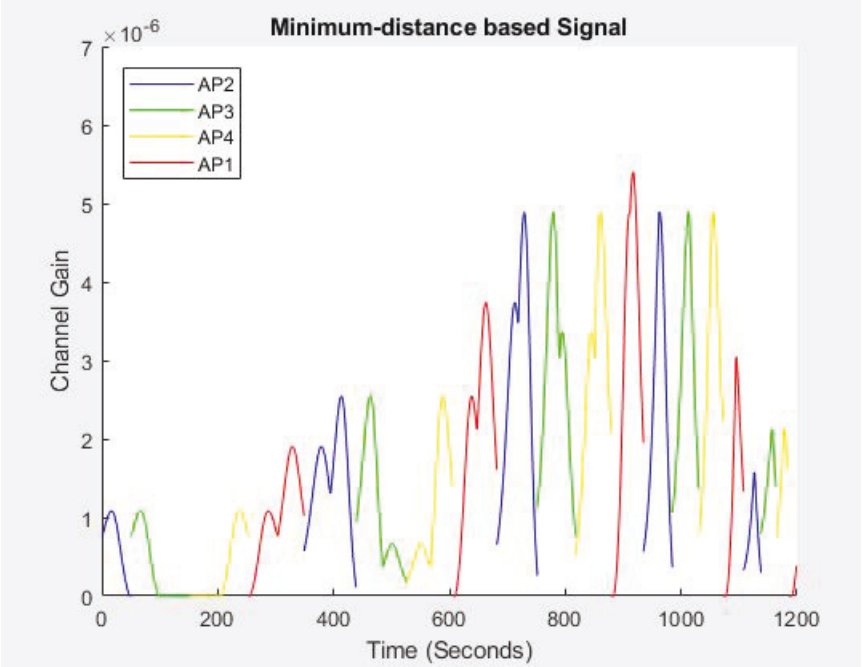

Figure 5.20 : Nearest-AP-based signal when $\alpha = 0$, $\beta = 0$ and $\gamma = 45^0$ [36].

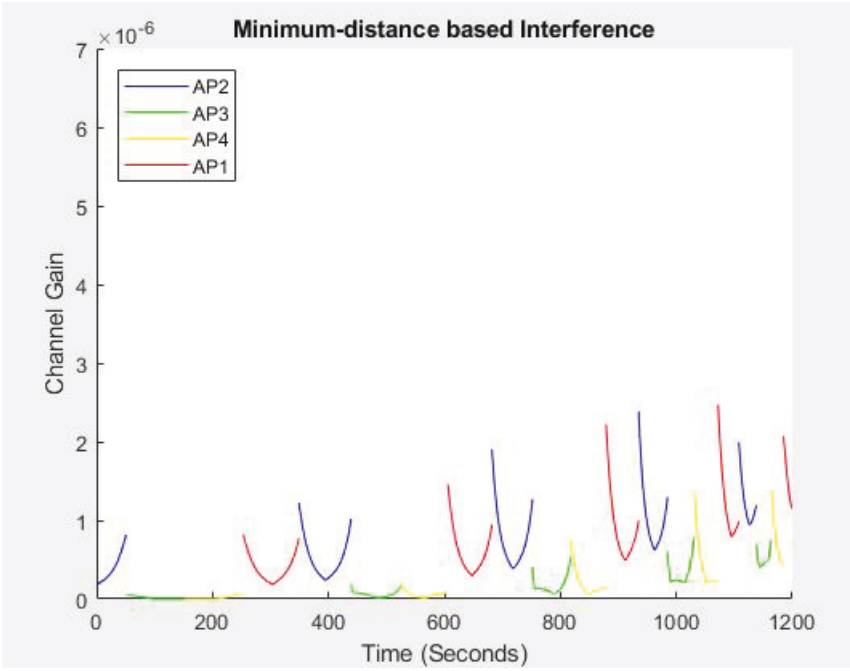

Figure 5.21 : Nearest-AP-based interference when $\alpha = 0$, $\beta = 0$ and $\gamma = 45^0$ [36].

Table 5.12 : Channel gain statistics of nearest-AP-based handover decision when $\alpha = 0$, $\beta = 0$ and $\gamma = 45^0$ [36].

Nearest-AP-based handover	Maximum	Minimum	Mean	Standard deviation
Gain value (10^{-6})	4.89	0	0.175	0.939
Interference value (10^{-6})	2.6	0	1.11	1.42
SIR (dB)	51.22	0	0.07	10.88

When the angles of β and γ increase to 80^0, the difference in level could be seen in from Fig. 5.22 to 5.25. For the two cases: $\beta = 80^0$, $\gamma = 0$ and $\beta = 0$, $\gamma = 80^0$ ($\alpha = 0$), the pattern of signal and interference is same. However, the values in the second case ($\alpha = 0$, $\beta = 0$ and $\gamma = 80^0$) are moved 70 seconds forward compared to the first case ($\alpha = 0$, $\beta = 80^0$ and $\gamma = 0$). Again, there is a discontinuity between serving channel gain values as the decision of choosing serving AP is based on the nearest distance between UE and APs.

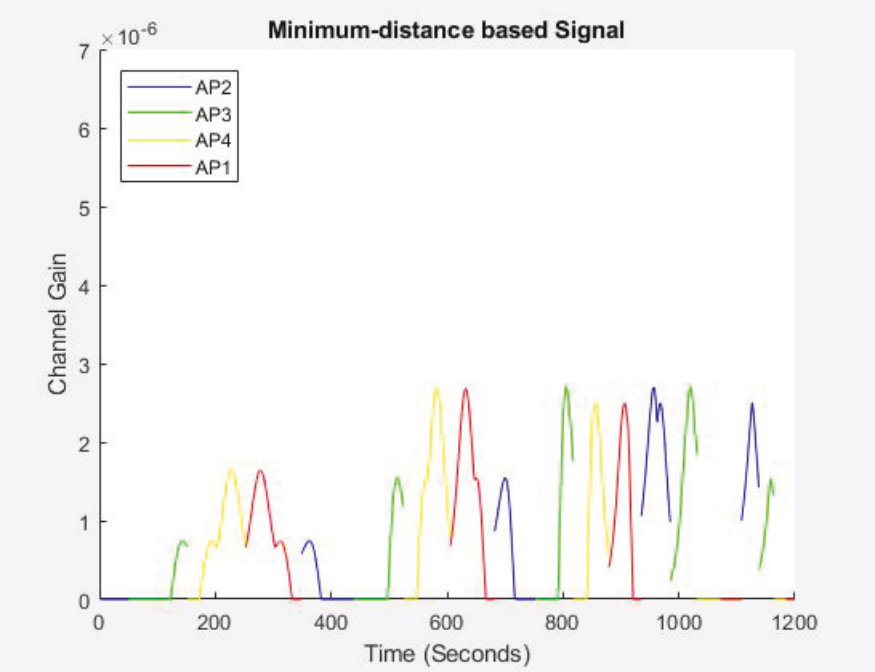

Figure 5.22 : Nearest-AP-based signal when $\alpha = 0$, $\beta = 80^0$ and $\gamma = 0$ [36].

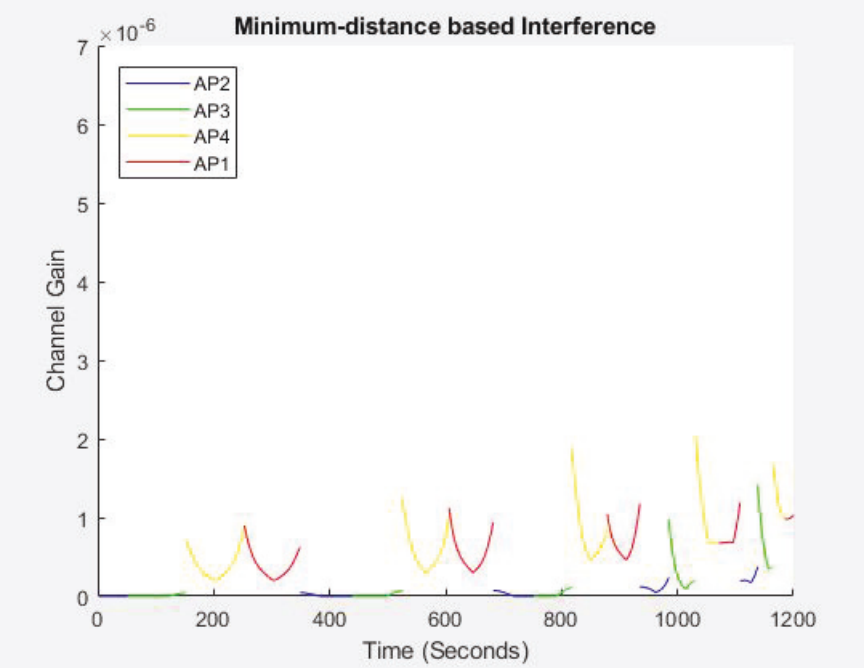

Figure 5.23 : Nearest-AP-based interference when $\alpha = 0$, $\beta = 80^0$ and $\gamma = 0$ [36].

For 70.08% of the time, there is no communication during this case: $\alpha = 0$, $\beta = 80^0$

and $\gamma = 0$ and 28.16% during this case: $\alpha = 0$, $\beta = 80^0$ and $\gamma = 0$ as the interference values are higher than received signal. However, the SIR values of second case is 7 times higher than that of the first case although the minimum and mean values are always 0 in both cases.

Table 5.13 : Channel gain statistics of nearest-AP-based handover decision when $\alpha = 0$, $\beta = 80^0$ and $\gamma = 0$ [36].

Nearest-AP-based handover	Maximum	Minimum	Mean	Standard deviation
Gain value (10^{-6})	2.68	0	0	0.539
Interference value (10^{-6})	1.98	0	0.686	0.807
SIR (dB)	6.61	0	0	1.33

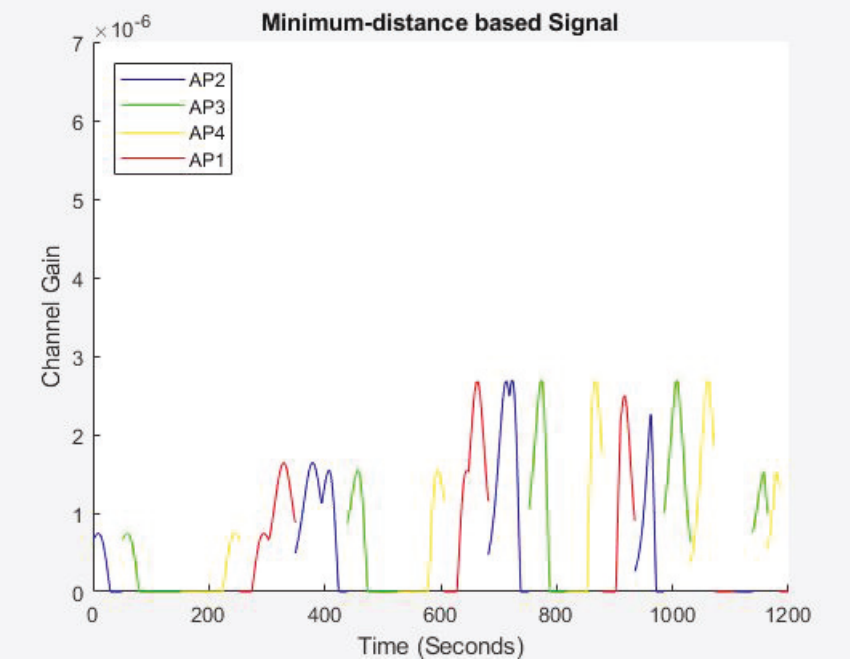

Figure 5.24 : Nearest-AP-based signal when $\alpha = 0$, $\beta = 0$ and $\gamma = 80^0$ [36].

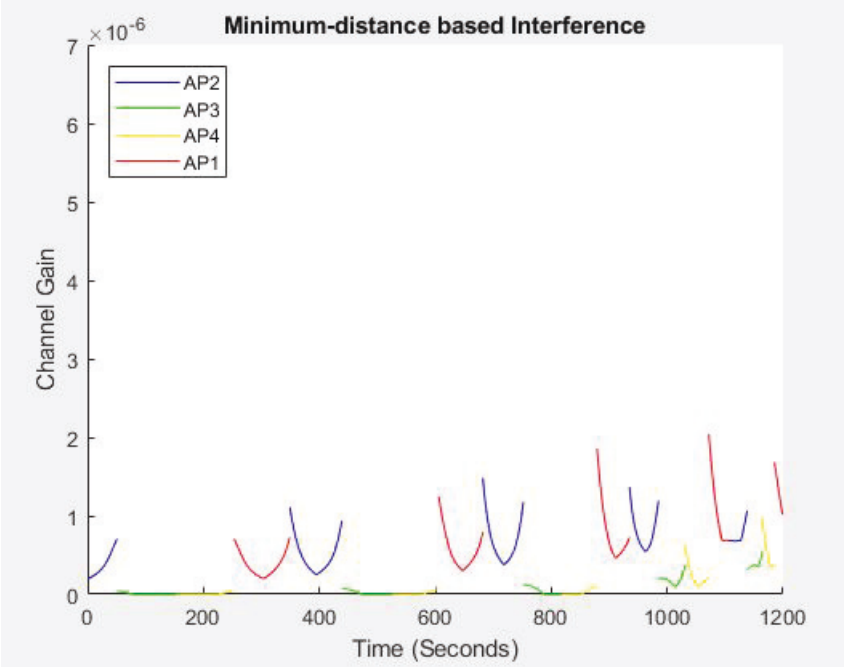

Figure 5.25 : Nearest-AP-based interference when $\alpha = 0$, $\beta = 0$ and $\gamma = 80^0$ [36].

Table 5.14 : Channel gain statistics of nearest-AP-based handover decision when $\alpha = 0$, $\beta = 0$ and $\gamma = 80^0$ [36].

Nearest-AP-based handover	Maximum	Minimum	Mean	Standard deviation
Gain value (10^{-6})	2.7	0	0.118	0.527
Interference value (10^{-6})	1.99	0	0.407	0.856
SIR (dB)	51.22	0	0	8.92

In summary, Fig. 5.16 and 5.17 show the signal and interference based on the minimum distance when UE is in normal direction. The serving AP is chosen if the distance between that AP and UE is minimal when compared to distance to the other three APs. It could be seen that the Signal to Interference ratio (SIR) is quite

low during the first quarter of the UE path. However, this ratio increased gradually in the remainder of the UE path. When the angles β and γ changed to 45^0, both signal and interference values are small (Fig. 5.18 to 5.21) due to the different transmission path between APs and photodetector. However, when these two angles are changed to 80^0 respectively, the SIR is quite high again. They are shown in the Fig. 5.22 to 5.25.

Channel gain values based on the nearest APs for indoor Li-Fi network was conducted in this part of the research. There was a discontinuity in the channel gain when there were the changes to the serving APs. The reason is the channel gain of serving APs based on the closest APs only. However, repeatedly, when user is moving closer to the center of the room where the high values of channel gain exist, the handover process performs better due to the large density of transmitted signals from four LEDs. And from the results, it also shows that the receiver rotation has a significant impact on the channel gain values when UE is moving around the network area.

5.4 Handover Assessment

Table 5.15 shows the statistics between two algorithms: the closest-AP-based and maximum-channel gain-based handover mechanism. Throughout the simulation interval, the UE is connected to AP1 for 24.38% of the time in which UE receives the maximum channel gain from AP1 and AP1 is also the closest AP. Thus, in this simulation of maximum-channel-gain-based handover, the UE is connected to the nearest AP for 99.59% (24.38+25.21+25.21+24.79) of the time and for the remainder 0.41% of the time, the UE is connected to another AP which is not the closest AP. This could explain the performance improvement for the case of maximum channel gain based handover compared to the case of nearest AP based handover [36].

Table 5.15 : Handover comparison between two handover decisions when $\alpha = 0$, $\beta = 0$ and $\gamma = 0$ [36].

	Minimum-distance-based Handover				
Maximum-channel gain-based handover	**AP1**	**AP2**	**AP3**	**AP4**	**Total**
AP1	24.38%	0%	0%	0%	**24.38%**
AP2	0.41%	25.21%	0%	0%	**25.62%**
AP3	0%	0%	25.21%	0%	**25.21%**
AP4	0%	0%	0%	24.79%	**24.79%**
Total	**24.79%**	**25.21%**	**25.21%**	**24.79%**	**100%**

Table 5.16 shows the statistics for the case of $\beta = 45^0$ where the UE is connected to the nearest AP for only 5.79% of the time and for the remainder 94.21% of the time, the UE is connected to another AP which is not the closest AP. From that we could see that UE's rotation affects its channel gain as well as handover decisions [36].

Table 5.16 : Handover comparison between two handover decisions when $\alpha = 0$, $\beta = 45^0$ and $\gamma = 0$ [36].

	Minimum-distance-based Handover				
Maximum-channel gain-based handover	**AP1**	**AP2**	**AP3**	**AP4**	**Total**
AP1	0%	0%	20.74%	5.7%	**24.38%**
AP2	24.79%	5.79%	4.46%	0%	**25.62%**
AP3	0%	0.33%	0%	19.09%	**25.21%**
AP4	0%	19.09%	0%	0%	**24.79%**
Total	**24.79%**	**25.21%**	**25.21%**	**24.79%**	**100%**

5.5 Conclusion

In this chapter, the simulation results of the single beam LEDs model are presented by considering the channel gain assessment, maximum-channel-gain-based handover decision, nearest-AP-based handover decision and handover assessment.

Over the mentioned-above assessment, the maximum-channel-gain-based handover decision outperforms the nearest-AP-based handover decision in terms of SIR values and the available communication period of time.

Chapter 6

Performance Analysis of Multiple Beams LEDs Model

In this chapter, the results of performance analysis of multiple beams LEDs are presented.

6.1 Channel Gain Assessment

The six beam angles of LEDs that have been chosen are (see Table 6.1): 0^0, 15^0, 30^0, 45^0, 60^0 and 75^0 in compute the received signal strength and interference of UE while moving around the test area.

Table 6.1 : Beam angle values [38].

Case number	Beam angles
1	0^0
2	15^0
3	30^0
4	45^0
5	60^0
6	75^0

When the beam angle is 0^0 (see Fig. 6.1 & 6.2), the channel gain of the four beams does not interfere with each other because all beams are facing down from the ceiling.

This also applies in the case when the beam angle is 15^0. However, at small angles, there are large coverage gaps which will reduce the achievable data rates for users. .

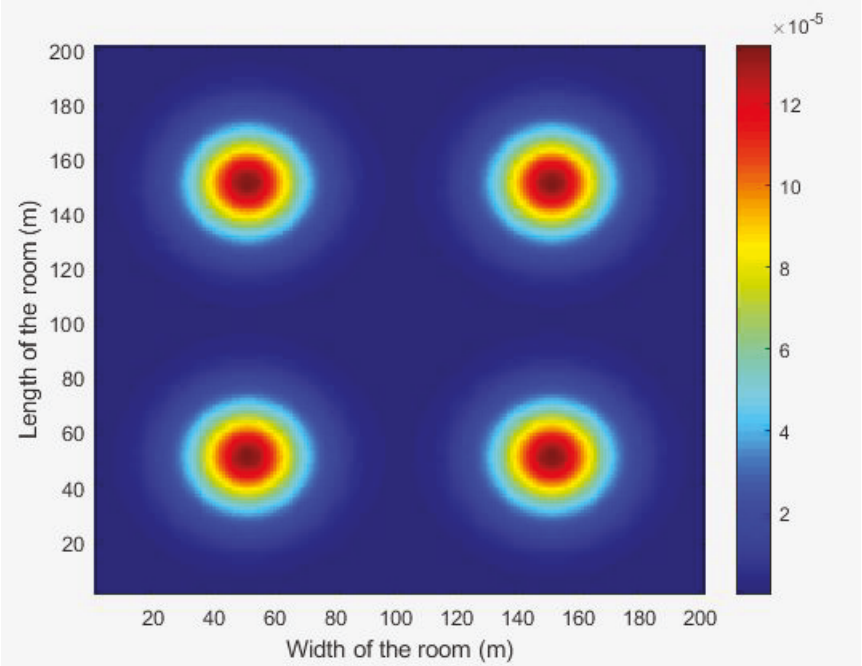

Figure 6.1 : Channel gain of multiple beams Li-Fi network (2D plot) when the beam angle is 0^0 [38].

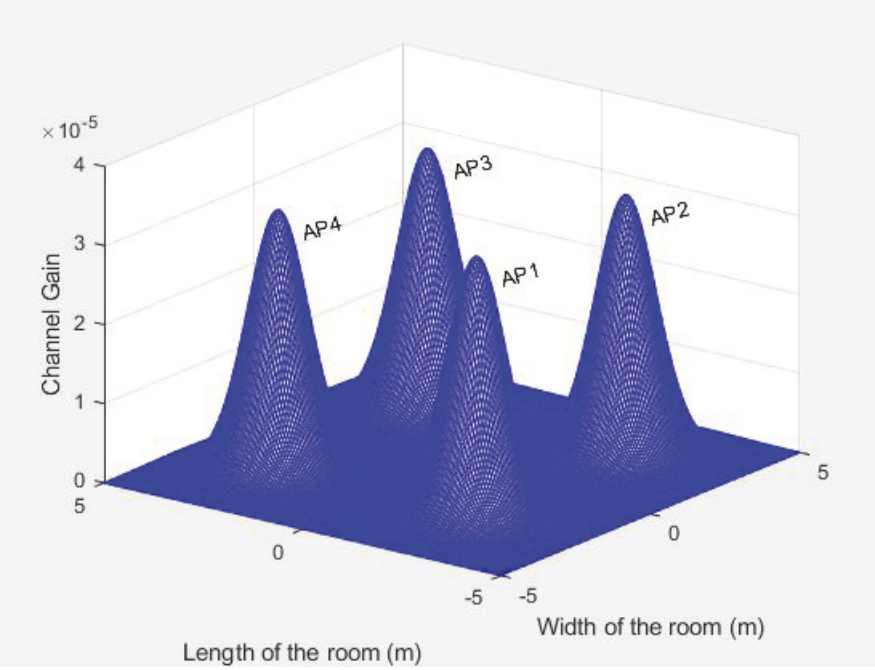

Figure 6.2 : Channel gain of multiple beams Li-Fi network (3D plot) when the beam angle is 0^0 [38].

When the beam angle is 15^0 (Fig. 6.3 & 6.4), there is little or no interference between four LEDs due to the small beam angle.

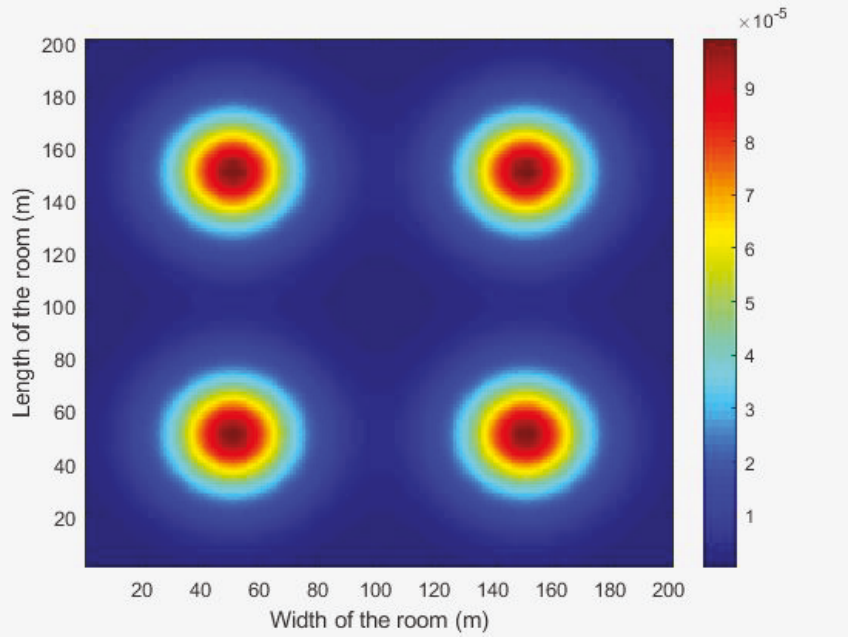

Figure 6.3 : Channel gain of multiple beams Li-Fi network (2D plot) when the beam angle is 15^0 [38].

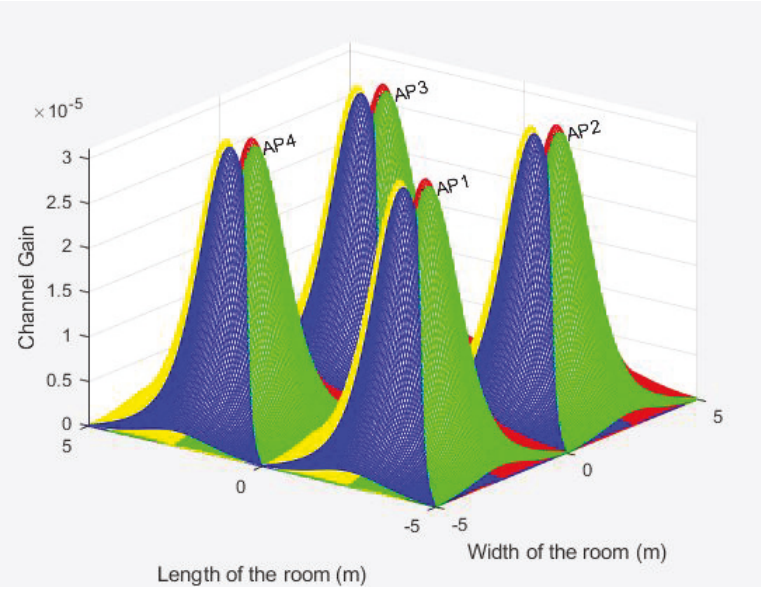

Figure 6.4 : Channel gain of multiple beams Li-Fi network (3D plot) when the beam angle is 15^0 [38].

When the beam angle is 30^0 (Fig. 6.5 & 6.6), there is some interference between

four beams from four LEDs. Also the network coverage has increased where 50% the room area has the channel gain more significant than 1.5 x 10^{-5}

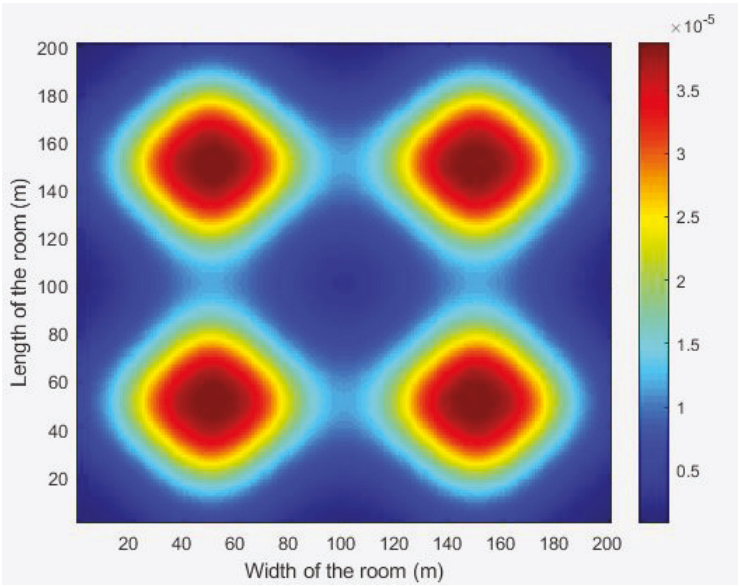

Figure 6.5 : Channel gain of multiple beams Li-Fi network (2D plot) when the beam angle is 30^0 [38].

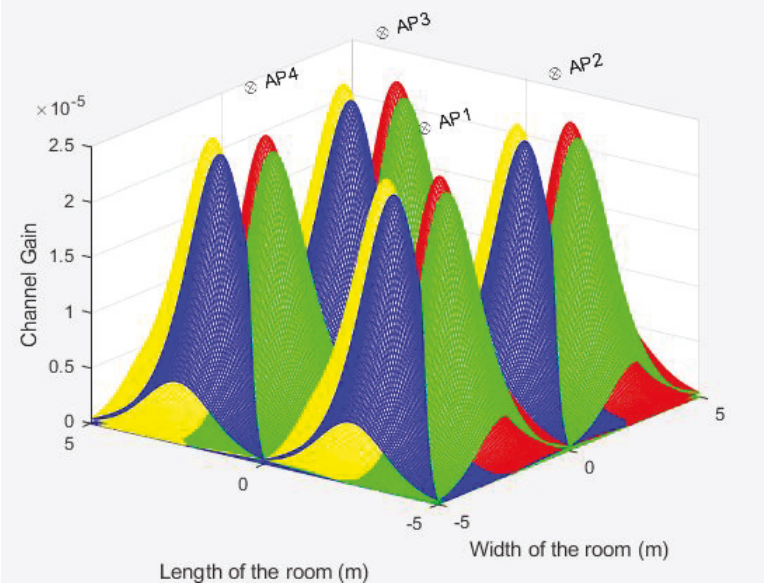

Figure 6.6 : Channel gain of multiple beams Li-Fi network (3D plot) when the beam angle is 30^0 [38].

When the beam angle is 45^0 (see Fig. 6.7 & 6.8), the interference between all 16 beams of the Li-Fi network is recognizable.

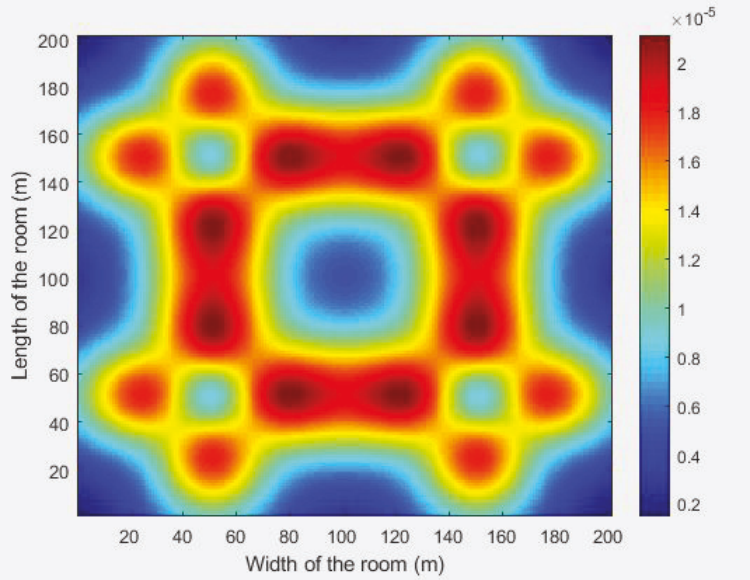

Figure 6.7 : Channel gain of multiple beams Li-Fi network (2D plot) when the beam angle is 45^0 [38].

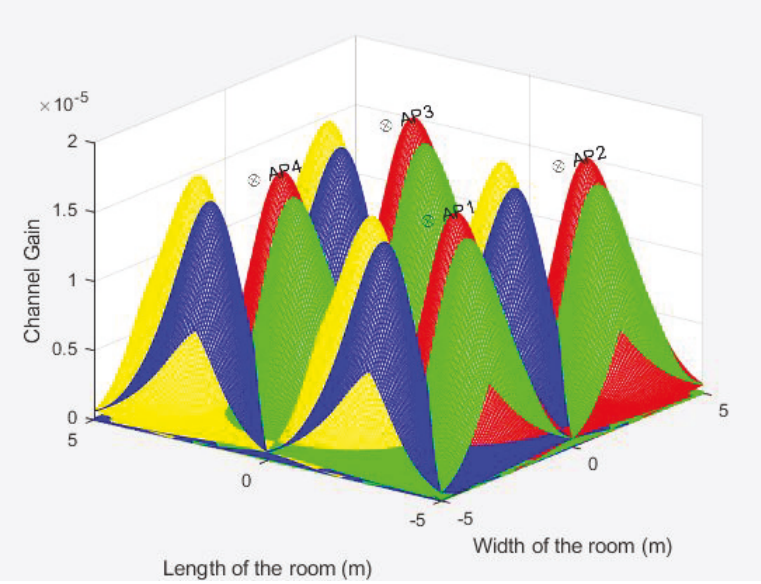

Figure 6.8 : Channel gain of multiple beams Li-Fi network (3D plot) when the beam angle is 45^0 [38].

When the beam angle is 60^0 (Fig. 6.9 & 6.10), the interference between all 16 beams of the Li-Fi network is much higher than the previous case of beam angle of 45^0.

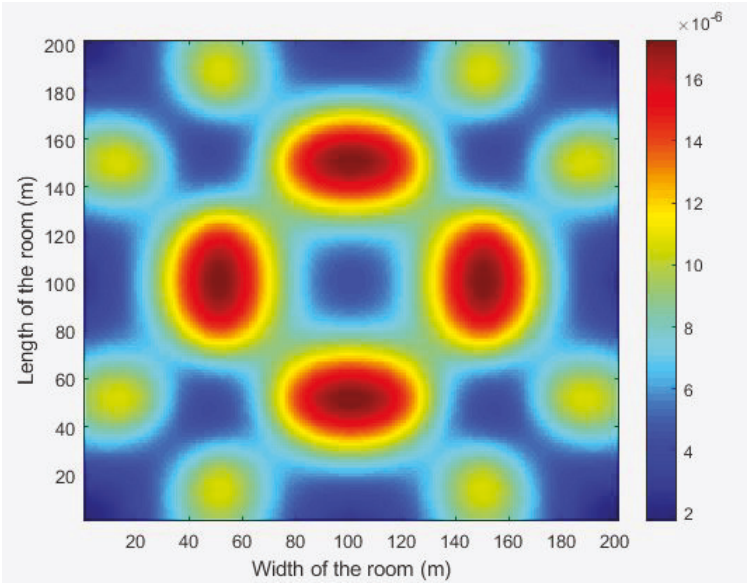

Figure 6.9 : Channel gain of multiple beams Li-Fi network (2D plot) when the beam angle is 60^0 [38].

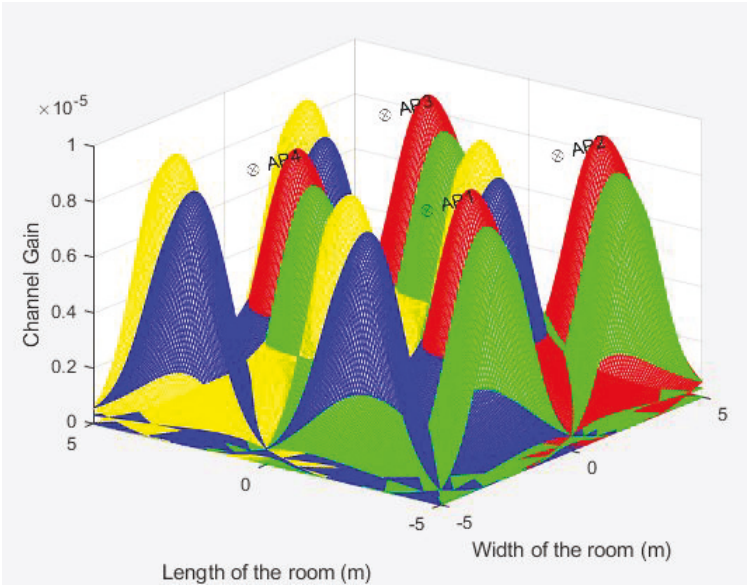

Figure 6.10 : Channel gain of multiple beams Li-Fi network (3D plot) when the beam angle is 60^0 [38].

When the beam angle is increased from 60^0 to 75^0 (Fig. 6.11 & 6.12), it is seen that the interference is much more severe from each beam of each LED.

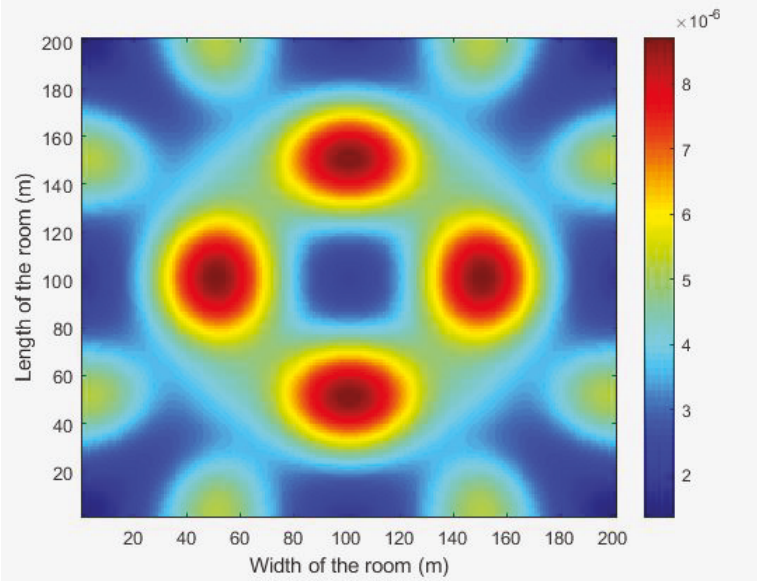

Figure 6.11 : Channel gain of multiple beams Li-Fi network (2D plot) when the beam angle is 75^0 [38].

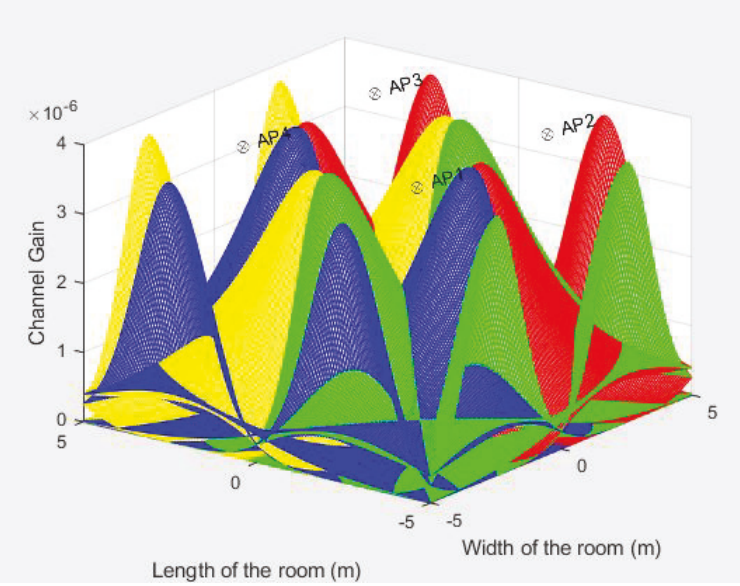

Figure 6.12 : Channel gain of multiple beams Li-Fi network (3D plot) when the beam angle is 75^0 [38].

6.2 Beam Angle Assessment

For each beam angle (0, 15^0, 30^0, 45^0, 60^0 & 75^0), the statistics in Table 6.3 shows the percentage of time that UE has specific range of SIR value. It is seen that most of the time (during the 1200 seconds), UE has the SIR values between 0 and 11.5. The SIR values of UE are between 0.5 and 1 most of the time and accounts for 89.2%, 80.3%, 62.8%, 44.7%, 30.5% and 49.8% of the total moving time for the case of beam angles are 0^0, 15^0, 30^0, 45^0, 60^0 and 75^0, respectively.

Table 6.2 : Percentage of each Signal to Interference Ratio (SIR) range for each beam angle set [38].

SIR	0^0	15^0	30^0	45^0	60^0	75^0
$0.0 < \text{SIR} \leq 0.5$	1.7%	7.2%	7.9%	12.1%	25.8%	33%
$0.5 < \text{SIR} \leq 1.0$	89.2%	80.3%	62.8%	44.7%	30.5%	49.8%
$1.0 < \text{SIR} \leq 1.5$	1.3%	7.9%	8.1%	9.9%	15.8%	13.9%
$1.5 < \text{SIR} \leq 2.0$	1.9%	0%	6%	6.7%	13.2%	3.3%
$2.0 < \text{SIR} \leq 2.5$	1.3%	0%	4%	6%	8.8%	0%
$2.5 < \text{SIR} \leq 3.0$	0%	1.3%	4%	4.6%	1.3%	0%
$3.0 < \text{SIR} \leq 3.5$	1.3%	0%	2.6%	9.3%	1.3%	0%
$3.5 < \text{SIR} \leq 4.0$	1.3%	0%	0%	2.7%	3.3%	0%
$4.0 < \text{SIR} \leq 4.5$	1.3%	0%	0%	2%	0%	0%
$4.5 < \text{SIR} \leq 5.0$	0.7%	1.3%	0%	0%	0%	0%
$5.0 < \text{SIR} \leq 5.5$	0%	0%	0%	2%	0%	0%
$5.5 < \text{SIR} \leq 6.0$	0%	0%	1.3%	0%	0%	0%
$6.0 < \text{SIR} \leq 6.5$	0%	1.3%	0%	0%	0%	0%
$6.5 < \text{SIR} \leq 7.0$	0%	0.7%	0%	0%	0%	0%
$7.0 < \text{SIR} \leq 7.5$	0%	0%	0%	0%	0%	0%
$7.5 < \text{SIR} \leq 8.0$	0%	0%	0%	0%	0%	0%
$8.0 < \text{SIR} \leq 8.5$	0%	0%	1.3%	0%	0%	0%
$8.5 < \text{SIR} \leq 9.0$	0%	0%	0%	0%	0%	0%
$9.0 < \text{SIR} \leq 9.5$	0%	0%	0%	0%	0%	0%
$9.5 < \text{SIR} \leq 10$	0%	0%	0%	0%	0%	0%
$10 < \text{SIR} \leq 10.5$	0%	0%	0%	0%	0%	0%
$10.5 < \text{SIR} \leq 11$	0%	0%	1.3%	0%	0%	0%
$11 < \text{SIR} \leq 11.5$	0%	0%	0.7%	0%	0%	0%
TOTAL	100%	100%	100%	100%	100%	100%

In the case of beam angle of 30^0, the SIR values are distributed along the range from 0 to 11.5, result in the highest value of Standard Deviation (SD) (1.91) and the second highest of mean SIR (0.8), coming after the case of the beam angle is 45^0.

Over the six cases of different beam angle values, Table 6.2 shows the maximum, minimum, mean and standard deviation of SIR values when changing beam angles. When UE is being served by one light beam, the signals from the other three APs are considered as interference. The SIR values are calculated by using Equation (10).

Table 6.3 : Signal to Interference Ratio (SIR) of UE (User Equipment) when changing beam angles [38].

Beam angles	**Maximum**	**Minimum**	**Mean**	**Standard deviation**
0	4.2	0	0.2	0.7
15^0	6.2	0	0.3	0.9
30^0	11.4	0	0.8	1.91
45^0	5	0	0.9	1.2
60^0	3.5	0	0.7	0.8
75^0	1.2	0	0.2	0.3

Fig. 6.13 is the Probability Density Function of the data taken from Table 6.3, it is shown that the SIR values when the beam angles are 0^0, 15^0, 45^0, 60^0 & 75^0 have its standard deviation smaller than the beam angle of 30^0 (grey colour).

In addition, in the case of beam angle of 30^0, there is less interference between 16 beams of the Li-Fi network. Hence, a beam angle of 30^0 (grey colour) was chosen

due to the considerably higher values of SIR.

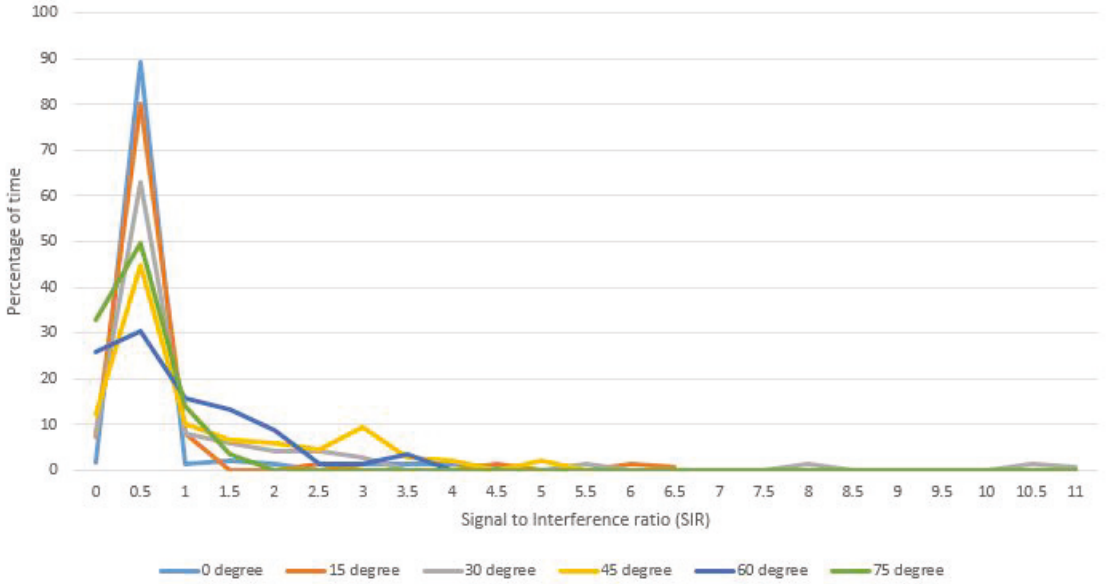

Figure 6.13 : Probability Density Function (PDF) when changing beam angles [38].

6.3 Conclusion

In this chapter, the simulation results of multiple beams LEDs model are presented by considering the channel gain assessment and beam angle assessment. The beam angle of 30^0 is recommended for the Li-Fi test network by considering the standard deviation and mean of SIR values. This chapter also presents a framework for assessing the performance of multiple beams Li-Fi network.

Chapter 7

Conclusions, Limitations and Future Research

In this chapter, we will summarise and conclude the research work presented in this thesis. The main findings are highlighted and conclusions are drawn. Finally, limitations and future work related to Li-Fi is presented.

7.1 Summary

The purpose of this thesis is to conduct modelling and simulation of the Li-Fi network (single beam and multiple beams).

In Chapter 1, the research topic was introduced by describing the demand for new wireless communications systems. Thereafter, I discussed the current research on Li-Fi which does not consider the movement of UE device in a single beam and multiple beams LEDs environment as well as impact of the beam angles in Li-Fi network system. After that, we listed two aims and three objectives for this research which are related to handover algorithms, handover process and SIR performance in Li-Fi. Next part of the thesis is three different research methods that are applied in this research: experimental, analytical and correlational methods which are followed by flowchart to describe the entire methodology of this research (models and simulations). Then layout of this thesis is presented to provide the general overview of this thesis and summary part is the last part of this chapter. This last part summarized the works had been done in the thesis.

In Chapter 2, the Li-Fi definition is described together with its history of development and evolution. In order to understand Li-Fi networks, the terms OWC, LED

bulbs and optical carriers are presented. In the history part, some OWC technologies were used in the past from different researchers are the fundamental approach for Li-Fi development in future. In the evolution part, the shortage of radio spectrum below 10GHz is mentioned leading to the commencement of new technology named Li-Fi - an optical version of Wi-Fi. Next, Li-Fi system operation and architecture are shown with an overview of Li-Fi network operation, transmitter and receiver chip, principle building blocks of Li-Fi and its application areas. In addition, the pros and cons of Li-Fi are also shown in the following part. The disadvantages of Li-Fi network are the limited range and short distance coverage of this network and compatibility with new Li-Fi enabled personal device. In terms of its advantages, Li-Fi uses LEDs bulbs for illumination and communication which is convenient and its high-security features. The descriptions of LAC network, downlink transmission and handover are presented in the next three parts. LAC network related to Li-Fi where LEDs are used as the AP. Only downlink transmission is considered in this research while assessing the handover process happened among the network and UE device.

In Chapter 3, the literature review is described by focusing on the handover algorithms, load balancing, multiple beams and intercell interference. Firstly, handover algorithms based on the AP selection algorithm in central controller unit to maximize the system throughput. Secondly, load balancing methods are used to maximize the proportional fairness index of all users, AP assignments and resource allocation and CSI. Next, multiple beams are also used to improve coverage areas by applying the angle diversity transmitter. Lastly, regarding the intercell interference, some studies such as Fourier analysis, the statistical-equivalent transformation of the SINR and the angle diversity receiver are used to provide a very close approximation to co-channel interference in attocell networks for both one and two dimensions, determine the coverage probability for saving energy and minimizing the co-channel

interference in multi-user Visible Light Communication (VLC) networks and mitigate interference, respectively.

In Chapter 4, modelling and simulation of the Li-Fi network are presented. The Li-Fi channel is described, including the Lambertian irradiance pattern and channel gain formulas. Next, the geometric orientation model is presented with the modelling of receiver orientation based on rotations around three axes. The Euclidean distance and optical concentrator of the receiver are also given in this part. In the next parts, the simulation model of spiral path is presented followed by the single beam and multiple beams LEDs models. In these two parts, the system configuration and simulation parameters are listed.

In Chapter 5, the simulation results of the single beam LEDs model are presented by considering the channel gain assessment, maximum-channel-gain-based handover decision, nearest-AP-based handover decision and handover assessment.

In Chapter 6, the simulation results of multiple beams LEDs model are presented by considering the channel gain assessment and beam angle assessment.

In conclusion, this dissertation provided the Li-Fi modelling and simulation for rotating and moving UE. In this case, we considered the single beam and multiple beams LEDs settings. Regarding to the single beam LEDs, two assessments are channel gain and handover is conducted. By evaluating two different algorithms: maximum-channel-gain-based and nearest-AP-based handover decision, we came up to the conclusion that the first mentioned-above handover outperforms the latter one by considering the SIR plus the time that communication is available. Regarding to the multiple beams LEDs, three different assessments are conducted including channel gain, UE signal and interference, and beam angles. For the beam angle assessment, by evaluating the SIR, UE has the highest SD and the second-highest mean when the beam angle is 30^0. That is the reason why the beam angle of 30^0

was chosen to match the Li-Fi system requirements.

7.2 Conclusions

The impact of UE rotation and movement are considered in this research for two types of handover decision: closest-AP-based and maximum-received-signal-based. Overall, we could see that maximum-received-signal-based handover decision performs better than closest-AP-based handover decision: the average channel gain value is 12.7 times larger for the normal case of UE's rotation (see Table 5.1 and 5.8) and 1.31dB higher for the case of $\beta = 45^o$ (see Table 5.3 and 5.10). The UE's rotation and movement also have some effects on handover decision causes the received signal to be reduced slightly; however, the percentage of possible communication to be degraded considerably: 8.69% for the handover decision based on maximum received signal (see Table 5.2 and 5.4) and 2.6 times lower for the handover decision based on closest AP (see Table 5.9 and 5.11) [36].

In addition, in the case of multiple beams LED environment, the beam angles and rotation of UE have some effects on UE channel gains. When the beam angle is 30^o, we could get the best value for SIR of 11.4, which is 1.5 times higher than in the other beam angles (see Table 6.3).

7.3 Limitations and Future Research

The multiple beams LEDs also consume much of the energy resources. Future research will focus on finding the best handover algorithm applied in Li-Fi multiple beams environment. In addition, we might focus on considering the effect of rotating UE in the multiple beams LEDs Li-fi network.

Bibliography

[1] CISCO 2016, *Cisco Visual Networking Index Global Mobile Data Traffic Forecast Update 2015 - 2020 White Paper*, viewed 07 August 2019, <https://bit.ly/3nXaqzO>

[2] C. Chen 2017, 'Downlink system characterisation in LiFi Attocell networks', Doctor of Philosophy Thesis, The University of Edinburgh.

[3] M. D. Soltani, H. Kazemi H., M. Safari and H. Haas, 'Handover Modeling for Indoor Li-Fi Cellular Networks: The Effects of Receiver Mobility and Rotation', *2017 IEEE Wireless Communications and Networking Conference (WCNC)*, San Francisco, CA, pp. 1-6.

[4] H. Haas, C. Chen and D. O'Brien 2017, 'A guide to wireless networking by light', *Progress in Quantum Electronics*.

[5] C. Barthold, K. P. Subbu, and R. Dantu 2011, 'Evaluation of Gyroscope Embedded Mobile Phones', *IEEE International Conference on Systems, Man, and Cybernetics*, pp. 1632-38.

[6] R. K. Penny and J. C. Gibbings 1974, 'The experimental method: a text for students of engineering and science', Longman, London.

[7] T. J. Quirk 2016, 'Excel 2016 for engineering statistics: a guide to solving practical problems'.

[8] V. T. David 2014, 'Research Methods for Engineers', Griffith University, Queensland.

[9] M. D. Soltani, X. Wu, M. Safari and H. Haas 2016, 'Access point selection in Li-Fi cellular networks with arbitrary receiver orientation', *IEEE* 27^{th} *Annual International Symposium on Personal, Indoor, and Mobile Radio Communications (PIMRC).*

[10] S. Dimitrov and H. Haas 2015, *Principles of LED Light Communications: Towards Networked Li-Fi*, Cambridge University Press.

[11] H. Haas 2013, *High-speed Wireless Networking Using Visible Light*, SPIE Newsroom.

[12] Z. Ghassemlooy, W. Popoola and S. Rajbhandari 2013,*Optical Wireless Communications: System and Channel Modelling with MATLAB (*1^{st} *edition)*, CRC Press.

[13] F. R. Gfeller and U. Bapst 1979, 'Wireless In-House Data Communication Via Diffuse Infrared Radiation', *Proceedings of the IEEE*, vol. 67, no. 11,pp. 1474-86.

[14] P. Barker and A. C. Boucouvalas 1998, 'Performance modeling of the IrDA protocol for infrared wireless communications, IEEE Commun. Mag., vol. 36, no. 12, pp. 113-7.

[15] European Commission 2008, *Technical briefing: Phasing out Incandescent Bulbs in the EU.*

[16] P. H. Pathak, X. Feng, P. Hu, and P. Mohapatra 2015, 'Visible light communication, networking, and sensing: A survey, potential and challenges', *IEEE Communications Surveys Tutorials*, vol. 17, pp. 2047-77.

[17] Z. Chen, D. A. Basnayaka, X. Wu and H. Haas 2018, 'Interference Mitigation for Indoor Optical Attocell Networks Using an Angle Diversity Receiver', *Journal of Lightwave Technology*, vol. 36, no. 18, pp. 3866-81.

[18] E. Sarbazi, M. Uysal, M. Abdallah, and K. Qaraqe 2014, 'Ray tracing based channel modeling for visible light communications', *2014* 22^{nd} *Signal Processing and Communications Applications Conference*, pp. 702-5.

[19] H. Haas, L. Yin, Y. Wang, and C. Chen 2016, 'What is LiFi?', *Journal of Lightwave Technology*, vol. 34, pp. 1533-44.

[20] A. Goldsmith 2005, *Wireless Communications*, Cambridge University Press.

[21] H. Elgala, R. Mesleh, and H. Haas 2009, 'Practical Considerations for Indoor Wireless Optical System Implementation Using OFDM', 10^{th} *International Conference on Telecommunications*, pp. 25-29.

[22] A. Yesilkaya, R. Bian, I. Tavakkolnia, and H. Haas 2019, 'OFDM-Based Optical Spatial Modulation', *IEEE Journal of Selected Topics in Signal Processing*.

[23] G. Miao, J. Zander, K. W. Sung, and S. B. Slimane 2016, *Fundamentals of Mobile Data Network*, Cambridge University Press.

[24] A. Ahmed, L. M. Boulahia, and D. Gaiti 2014, 'Enabling Vertical Handover Decisions in Heterogeneous Wireless Networks: A State-of-the-Art and A Classification', *IEEE Communications Surveys and Tutorials*, vol. 16, pp. 776-811.

[25] Z. Chen, D. A. Basnayaka, X. Wu and H. Haas 2018, 'Interference Mitigation for Indoor Optical Attocell Networks Using an Angle Diversity Receiver', *Journal of Lightwave Technology*, vol. 36, no. 18, pp. 3866-81.

[26] Y. Wang, D. A. Basnayaka, X. Wu and H. Haas 2017, 'Optimization of Load Balancing in Hybrid LiFi/RF Networks', *IEEE Transactions on Communications*, vol. 65, no. 4, pp. 1708-20.

[27] X. Wu, M. Safari and H. Haas 2017, 'Access Point Selection for Hybrid Li-Fi and Wi-Fi Networks', *IEEE Transactions on Communications*, vol. 65, no. 12,

pp. 5375-85.

[28] Y. Wang, X. Wu and H. Haas 2016, 'Fuzzy logic based dynamic handover scheme for indoor Li-Fi and RF hybrid network', *2016 IEEE International Conference on Communications (ICC)*, pp. 1-6.

[29] X. Wu, D. Basnayaka, M. Safari and H. Haas 2016, 'Two-stage access point selection for hybrid VLC and RF networks', *2016 IEEE 27th Annual International Symposium on Personal, Indoor, and Mobile Radio Communications (PIMRC)*, pp. 1-6.

[30] M. Dehghani Soltani, X. Wu, M. Safari and H. Haas 2016, 'Access point selection in Li-Fi cellular networks with arbitrary receiver orientation', *2016 IEEE 27th Annual International Symposium on Personal, Indoor, and Mobile Radio Communications (PIMRC)*, pp. 1-6.

[31] Z. Chen, D. A. Basnayaka and H. Haas 2017, 'Space Division Multiple Access for Optical Attocell Network Using Angle Diversity Transmitters', *Journal of Lightwave Technology*, vol. 35, no. 11, pp. 2118-31.

[32] H. Kazemi, M. Safari and H. Haas 2017, 'A wireless backhaul solution using visible light communication for indoor Li-Fi attocell networks', *2017 IEEE International Conference on Communications (ICC)*, pp. 1-7.

[33] A. Surampudi and R. K. Ganti 2018, 'Interference Characterization in Downlink Li-Fi Optical Attocell Networks', *Journal of Lightwave Technology*, vol. 36, no. 16, pp. 3211-28.

[34] L. Yin and H. Haas 2018, 'Coverage Analysis of Multiuser Visible Light Communication Networks', *IEEE Transactions on Wireless Communications*, vol. 17, no. 3, pp. 1630-43.

[35] V. K. Papanikolaou, P. P. Bamidis, P. D. Diamantoulakis and G. K. Karagiannidis 2018, 'Li-Fi and Wi-Fi with common backhaul: Coordination and resource allocation', *2018 IEEE Wireless Communications and Networking Conference (WCNC)*, pp. 1-6.

[36] H. D. Huynh, K. Sandrasegaran and S. C. Lam 2018, 'Modelling and Simulation of Handover in Light Fidelity (Li-Fi) Network', *TENCON 2018 - 2018 IEEE Region 10 Conference*, pp. 1307-12.

[37] A. Agarwal and G. Saini 2014, 'SNR Analysis for Visible Light Communication Systems', *International Journal of Enngineering Research and Technology (IJERT)*, vol. 3.

[38] H. D. Huynh and K. S. Sandrasegaran 2019, 'Coverage Performance of Light Fidelity (Li-Fi) Network', *2019* 25^{th} *Asia-Pacific Conference on Communications (APCC)*, pp. 361-66.

[39] H. Haas 2018, 'LiFi is a paradigm-shifting 5G technology', *Reviews in Physics 3*, pp. 26-31.

[40] V.J. RajaKumar and S. Bhuvaneshwari 2017, 'A Study on Li-Fi-Internet at the Speed of Light', *International Journal of Innovative Research in Computer and Communication Engineering*, vol. 5, issue 6.